

Copyright © 1981, by the author(s).  
All rights reserved.

Permission to make digital or hard copies of all or part of this work for personal or classroom use is granted without fee provided that copies are not made or distributed for profit or commercial advantage and that copies bear this notice and the full citation on the first page. To copy otherwise, to republish, to post on servers or to redistribute to lists, requires prior specific permission.

**EFFECTS OF RANDOM AND PERIODIC  
EXCITATIONS ON RELAXATION OSCILLATORS**

by

Asad Abidi

Memorandum No. UCB/ERL M81/80

28 September 1981

**EFFECTS OF RANDOM AND PERIODIC  
EXCITATIONS ON RELAXATION OSCILLATORS**

by

Asad Adibi

Memorandum No. UCB/ERL M81/80

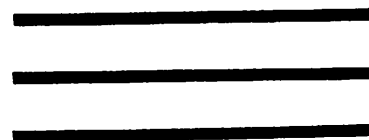
28 September 1981

**ELECTRONICS RESEARCH LABORATORY**

College of Engineering  
University of California, Berkeley  
94720

Effects of  
Random & Periodic  
Excitations on  
Relaxation Oscillators

by  
Asad Abidi



## **Abstract**

The cycle-to-cycle jitter produced by circuit noise sources in most relaxation oscillators severely limits their applications in telemetry and communications circuits. The mechanism of jitter production, a non-linear time-varying problem, has not been reported anywhere in the literature, and is the subject of this thesis. A model of this mechanism has been derived which applies to all relaxation oscillators, and, in fact, to noise in all regenerative circuits. Although the statistics of jitter are difficult to describe analytically, some very useful empirical results have been obtained. The criteria for the design of low jitter oscillators thus become evident, and have been used to demonstrate a prototype circuit with an order of magnitude less jitter than any commercial circuit.

Finally, as an extension of this model, the synchronisation and aperiodic dynamics of relaxation oscillators in the presence of periodic signals are investigated.

---

*To my dear mother and father,  
not just for their patience.*

"What human beings seek for is a unifying principle in this apparently chaotic universe; ...

The most common of these principles is science, which discovers (or creates) cause and effect. The trouble with science is that cause and effect are only too efficient as an explanation; there is no mystery, no wonder, no interest remaining ...

The most remarkable, and most unexpected, of all these principles is nonsense.

Nonsense does not mean no sense whatever; it implies a sense which is imperceptible by the reason, and can be assumed and justified only by an experience of that very "sense", that is, nonsense. There is a super-natural order, in which there is no intellect, no emotion, no beauty, no morality, no unifying principle, no order of any kind, natural or super-natural."

*R.H. Blyth, ZEN & ZEN CLASSICS.*

Designed and produced by the author.

Set in Times Roman using

the UNIX typesetting facilities

at the U.C.Berkeley Computer Centre.

## Acknowledgements

It is with pleasure that I acknowledge the following:

Professor R.Meyer, my research advisor, for initiating this study and giving it his constant guidance; for motivating me in periods of lull while granting me complete independence the rest of the time; for faithfully supporting me as a research assistant; but most of all, for his genial sense of humour.

Professor D.Hodges, for his generous support, financial and otherwise, which he gave without hesitation whenever the need arose.

My fellow students of the past few years, Bill Black in particular, who were also my teachers. Cynthia, Ann and Doris, for making up in many ways for an otherwise very masculine department.

This work was done under the U.S. A.R.O. Grant DAAG29-80-K-0067.

---

## TABLE OF CONTENTS

Prologue	1
<b>Chapter 1</b>	
Oscillators: Harmonic and Relaxation	4
<b>Chapter 2</b>	
Noise in Relaxation Oscillators: Characterisation and Measurement	17
<b>Chapter 3</b>	
A Theory of Jitter in Relaxation Oscillators	25
<b>Chapter 4</b>	
The Statistics of Phase Jitter	51
<b>Chapter 5</b>	
Low Jitter Oscillator Circuits	68
<b>Chapter 6</b>	
Synchronisation in Relaxation Oscillators	77
References	95
Appendix 1	98
Appendix 2	100

---

## Prologue

Relaxation oscillators belong to a most useful, yet quite mysterious class of electronic circuits. If one were to attempt a classification of commonly used circuits by intricacy of their dynamical behaviour, it would probably resemble the following: Passive circuits, like resistors, capacitors and inductors; Transistor amplifiers without feedback; Sinusoidal, single frequency, oscillators; Amplifiers with negative feedback; and Relaxation Oscillators. It is interesting to note that the last two categories were discovered at about the same time, and have engaged the interest of theoreticians and engineers since. Relaxation oscillators have come to the fore recently because of a renaissance of interest in the dynamics of the van der Pol oscillator [1], and of the widespread need for multivibrators with voltage-controllable frequency of oscillation for use in integrated circuit Phase Locked Loops [2].

Relaxation oscillators have certain other properties which makes them eminently suitable as a workhorse in signal generation. They require only one timing element, which need not be an expensive selective element like a quartz crystal or an L-C circuit; the amplitude of oscillation is easily adjustable; and the frequency of oscillation can be swept over four decades or more by electronic control without changing the timing element. A versatile circuit like this is not without its attendant problems, foremost of which are drift and noise. Whereas a quartz crystal has a natural insensitivity to temperature and other environmental factors, the frequency of a relaxation oscillator can have a very large temperature coefficient, because it is directly determined by active device parameters, like the ON voltage of a diode. The problem is not insurmountable, as is demonstrated by recent designs [3], where temperature dependent currents are used for compensation. Again, a highly frequency selective circuit has a natural filtering effect on broadband noise, so reducing its presence on the periodic output, whereas a relaxation oscillator is essentially a broadband circuit, with no frequency limitations other than the maximum frequency response of its active devices. Thus, it is susceptible to all forms of noise in the frequency spectrum, which, manifested on the output waveform, produce a

---

random modulation of the oscillation's period known as the Phase Jitter.

It is appropriate here to point out the essential differences between a Sinusoidal oscillator and a Relaxation oscillator. The former relies on the frequency selectivity of a tuning element to generate a single frequency. More precisely, the sharp rolloff of the phase characteristic of the tuning element as a function of frequency is used in a feedback loop to satisfy the Nyquist criterion for instability. At least two independent energy storages are necessary to produce the desired phase characteristic in the timing element, that is, the system must at least be second order for oscillation. The amplitude of oscillation is determined by the limiting characteristics of the loop, produced by the non-linear active elements in the circuit. This, in turn, produces distortion in the oscillation, which is minimised by ensuring "softness" in the limiting [4].

A relaxation oscillator is best described by analogy with the sinusoidal oscillator. If one of the energy storages is reduced in value so that it becomes of the order of the parasitic elements in the circuit, the dynamics of the circuit will significantly change from those during the sinusoidal operation. The phase criterion will no longer be satisfied at a single frequency, yet a highly non-sinusoidal oscillation will exist, whose frequency and amplitude both will be determined by the large scale limiting behaviour of the circuit, and by the magnitude of certain crucial currents and voltages. The oscillation cycle will typically consist of a fast transition between two stable states, and a slow energy input period during which the circuit is said to be "relaxing", whence the name. There are certain provisos to this analogy, discussed in CHAPTER 1 , but, roughly speaking, it is merely a degenerate sinusoidal oscillator.

There are other forms of oscillators and oscillations which could be classified as the relaxation type; the above discussion should be regarded as a simplified prototype for most of them.

A broadband circuit like a relaxation oscillator is strongly influenced by noise. The Phase Jitter so produced sets a limit on the usefulness of the circuit as a frequency detector in a Phase Locked Loop, for clearly it cannot resolve frequency shifts less than the jitter. In practice, this is often the major limitation in using the oscillator. Yet, there exists no theory for determining the effect of noise on such non-linear, time-varying circuits, and consequently no systematic

---

circuit design methods to reduce its effects.

The central object of this study has been to develop, and verify, such a theory of Phase Jitter in relaxation oscillators, and examine its implications on circuit design.

---

# C H A P T E R 1

---

## Oscillators: Harmonic and Relaxation

The desire to generate periodic signals has existed throughout the history of electronics, principally motivated by radio applications. Early oscillators were of the *harmonic* type, where the energy exchange properties of two coupled reactive elements were used, as an analogue to the simple pendulum, to produce a simple harmonic oscillation of electromagnetic energy. A charged lossless capacitor,  $C$ , when discharged into a lossless inductor,  $L$ , will produce a sinusoidal oscillation of voltage and current of frequency  $(LC)^{-1/2}$ . In the presence of dissipation, the resulting oscillation has a decaying amplitude. Oscillation is sustained by using an active circuit to make up for the dissipation in each cycle.

The presence of the active circuit necessarily results in a steady state oscillation different than a sinusoidal one. The operation of this circuit is as follows: it provides a dynamic negative resistance slightly in excess of the dissipation of the reactive elements used for tuning, and limits the resulting oscillation of growing amplitude by reverting to a positive resistance at some pre-determined voltages. The steady state oscillation amplitude balances the energy input by the nett negative resistance per cycle, with the dissipation. The methods of harmonic oscillator design are well documented [4],[5], and it is possible to obtain an impressively low distortion in the output by careful design <sup>1</sup>.

Harmonic oscillators where the *lumped* circuit assumptions above are true can typically produce frequencies upto many megahertz. Beyond this range, from microwaves to X-rays,

<sup>1</sup>However, there appears to be a tradeoff in the design of stable (over time) and low distortion (spectrally pure) oscillators, e.g. the HP 10811 uses a quartz crystal to attain a stability of  $10^{-10}$  parts/day, while the HP 239A uses a Wien bridge to produce total harmonic distortion of -95 dB, with much worse stability.

oscillators rely on the physical properties of suitable resonant cavities to sustain stationary waves, and cannot strictly be called electronic circuits. For example, lasers operating in the infrared wavelengths and beyond, although harmonic oscillators, are *distributed* oscillators from the circuit point of view, and not of direct interest in this study <sup>2</sup>.

A typical harmonic oscillator circuit is shown in Fig.1.1 (a), which uses an L-C tank circuit for frequency selection, and bipolar transistors as active devices. These devices simulate the limited negative resistance of Fig. 1.1 (b). The steady-state oscillation defines a closed cycle in the phase plane of Fig. 1.1 (b), where time is a parameter on the trajectory. Such a circuit can be generically, and concisely, represented by the differential equation that van der Pol originally studied[1]:

$$\ddot{x} + \lambda(1 - \mu x^2)\dot{x} + \omega^2 x = 0 \quad (1.1)$$

where  $\lambda, \mu$  are determined by the degree of limiting in the negative resistance, and  $\omega$  is the frequency of oscillation for small  $\lambda$ .

This study concerns itself with the effects of circuit noise on the output waveform. For harmonic oscillators, this is a well studied problem, motivated originally in the 1950's by the need to make precise electronic clocks for high resolution applications like Doppler radar[6]. These results are now summarised.

### Harmonic Oscillator noise

The earliest attempt at understanding the effects of noise in harmonic oscillators was made by Stewart in 1956[7], where he extended the results of modulation theory to the physical

<sup>2</sup> It is often desirable to model the operation of a distributed oscillator by an electronic circuit analogue. The frequency of oscillation must be scaled accordingly.

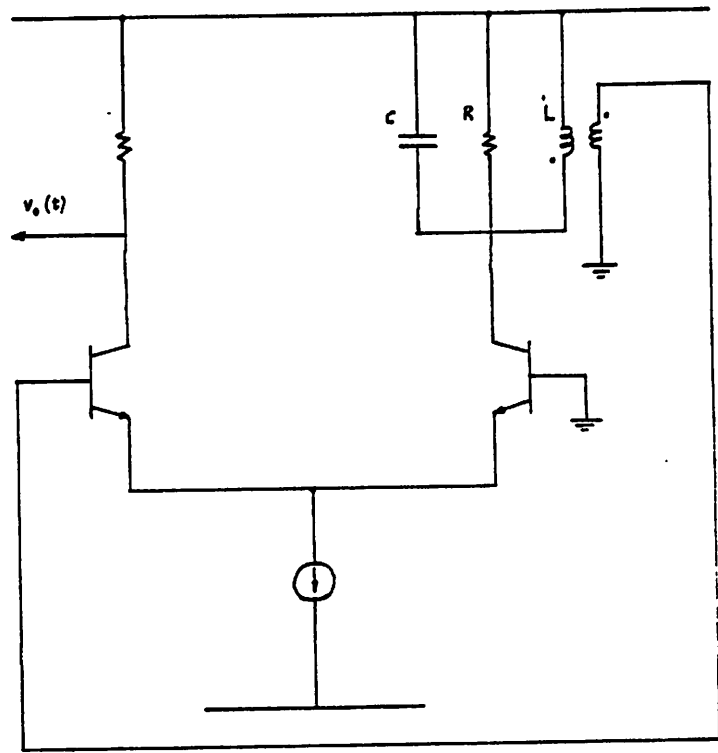


Fig. 1.1(a)

An L-C oscillator circuit using bipolar transistors

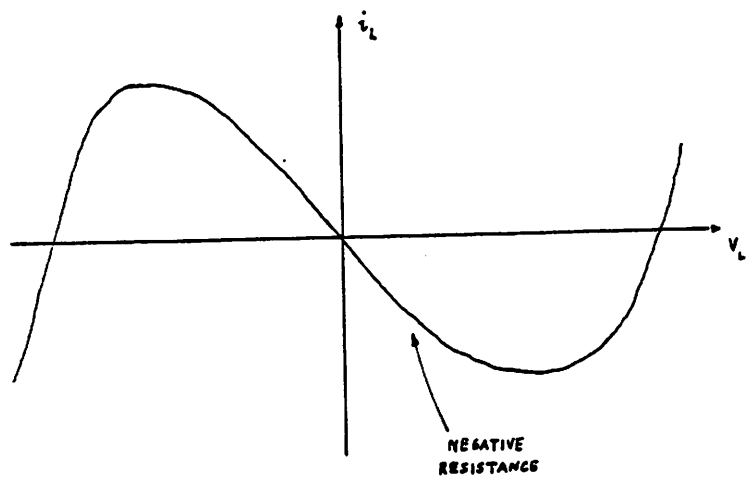


Fig. 1.1(b)

Negative resistance characteristics produced by active devices

processes of noise in oscillator circuits. Low-pass filtered white noise, after modulating a sinusoidal carrier, produces sidebands around the carrier (Fig. 1.2). The *bandwidth* of these sidebands is proportional to the *noise density*; this was the central result of the paper, from which the sideband power could be calculated.

Edson [8] attacked the same problem in a slightly different manner, by considering the noise as randomly spaced impulses exerting a *synchronising* influence on the oscillator. His results were similar to Stewart's, with the noise sidebands given by

$$v^2(\omega) = \frac{2kT G}{\left[ \frac{\omega_0^2 CkT}{2PQ^2} \right]^2 + 4C^2(\omega - \omega_0)^2} \quad (1.2)$$

where

$G$  = loss conductance of tank circuit

$\omega_0$  = oscillation frequency

$C$  = capacitance in tank circuit

$P$  = oscillator output power

$Q$  = quality factor of tank circuit

Simplified calculations such as these assume that the loss resistance is the only source of noise, and hence determines the noise density at  $\omega = \omega_0$ . The total noise power in the sidebands then depends on their -3dB bandwidth and from (1.2) it is evident that this varies inversely with  $P$  and  $Q$ . Therefore, for low noise, a large oscillation amplitude and high  $Q$  are necessary.

The other important analyses by Mullen [9], Golay [10] and Grivet & Blaquiére [11] arrive at slight variations of the same basic results. They set up simple models of the active circuit associated with the tank circuit, and calculate the noise vector which adds to the steady state oscillation vector. The noise vector may be resolved into its in-phase and quadrature components, and while the in-phase component results in a random amplitude modulation, the quadrature component produces phase noise. The results for the phase noise spectrum are as

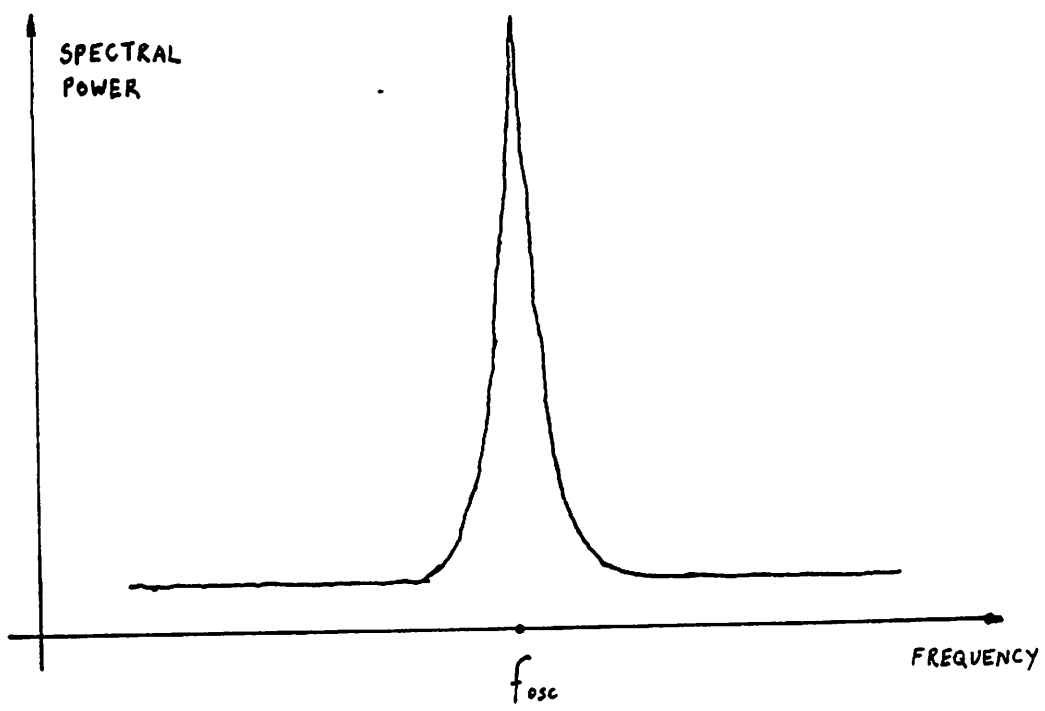


Fig. 1.2

Noise sidebands around the frequency of oscillation

follows:

$$\text{[Mullen]} \quad \text{Noise bandwidth} = \frac{kT R^3 \omega_0^2}{Q^2 P} \quad (1.3)$$

$$\text{[Golay]} \quad \text{Noise bandwidth} = \frac{\omega_0}{2\pi Q} \sqrt{\frac{2kT \omega_0}{PQ}} \quad (1.4)$$

$$\text{[Grivet]} \quad \text{Noise bandwidth} = \frac{kT \omega_0^2}{\pi P Q^2} \quad (1.5)$$

All these formulae show the same dependence of the noise bandwidth on the oscillator variables as (1.2).

The magnitude of the noise bandwidth is much smaller than the -3dB bandwidth of the dissipative tank circuit. For example, for typical values of  $Q = 10^6$ ,  $\omega_0 = 10$  Mrad/s, and  $P = 10 \mu\text{W}$ , the effective noise bandwidth of the oscillator is  $10^{-14}$  rad/s while the -3dB bandwidth of the tank circuit is 10 rad/s. This is because the active circuit raises the effective  $Q$  of the tank to a very large value in order to sustain oscillation, and ultimately the  $Q$  is bounded above by the presence of noise. For the previous values, the circuit  $Q = 10^{21}$ .

For precise frequency applications, it is important that the spreading of the oscillator line spectrum be kept to a minimum. A low phase noise oscillation can also be used for precise *timing* where the instants when the waveform crosses its mean value (hereafter assumed zero) are used as a clock to measure time. While the phase noise sidebands are obtained by a linear (Fourier) transformation of the noisy waveform, the zero-crossing instants result from a non-linear transformation. Phase noise produces a *jitter* in the periodicity of the zero-crossing times. The jitter can be calculated knowing the noise bandwidth. If the noise density at the centre frequency is  $4kTR \text{ V}/\sqrt{\text{Hz}}$  and the noise bandwidth is  $B$ , then the total noise voltage in quadrature is  $4kTR\sqrt{B}$  V. At the instant of zero crossing, this produces an uncertainty in time given by

$$\delta t = \frac{4kTR\sqrt{B}}{\text{Slope of oscillation at crossing}}$$

---

This is explained in Fig.1.3, where the noise is represented as random variations in the mean value. As the noise power is bunched around the oscillation frequency, these variations are slow compared to the latter.

### Relaxation Oscillators

Relaxation oscillators developed independently of sinusoidal oscillators, evolving from the cross-coupled trigger circuit of Eccles and Jordan (1919) [12]. The principle is described in block diagram form in Fig.1.4, where an energy storage is charged through a valve from a power supply, and when the stored energy exceeds an upper threshold, a rapid discharge results, whence the cycle repeats, resulting in a sawtooth periodic waveform. There are various practical realisations of this idea, and a triangle wave can be produced if a symmetrical scheme is used.

According to the theory of dynamical systems, a system must at least be second-order to oscillate. How can a relaxation oscillator work with only one energy storage? The operation can be explained if the parasitic elements are considered. In any real circuit, small parasitic elements will exist which increase the order of the system. Normally, in a *robust* system, the parasitics do not qualitatively change the dynamics, but a relaxation oscillator is a *degenerate* system, where the parasitics solely determine part of the oscillation. The phase plane diagram for the steady state relaxation oscillation is shown in Fig.1.5. Although it resembles the van der Pol cycle, there are two time scales to this motion: a slow charging governed by the energy storage, and a fast transition determined by the parasitics.

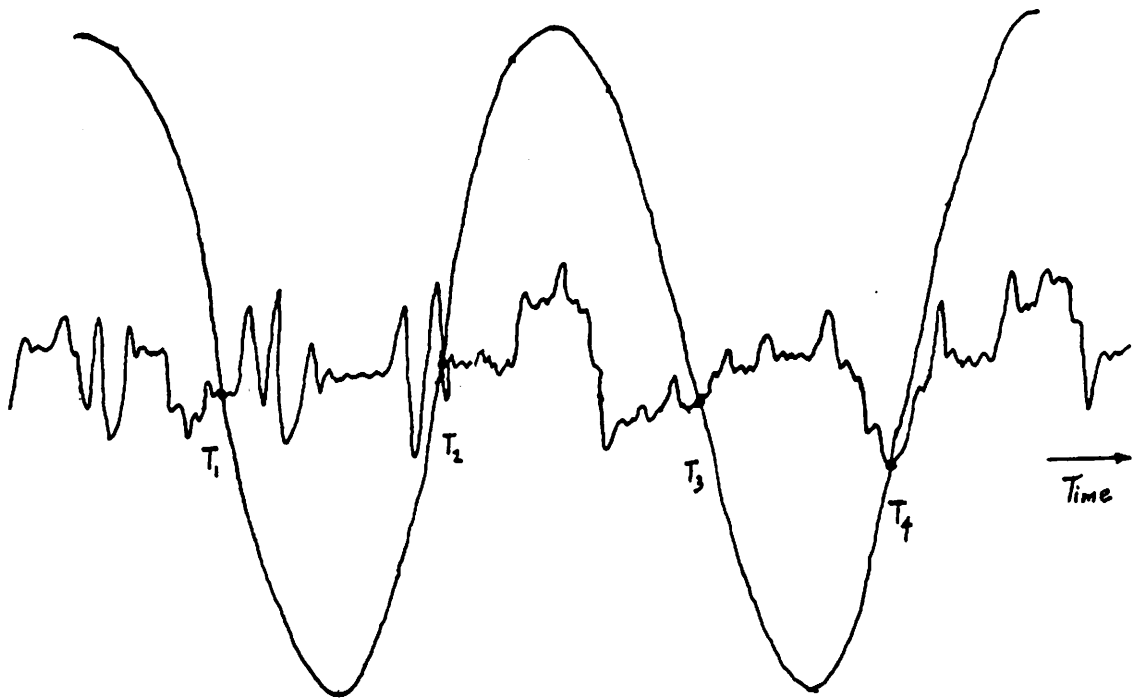


**Fig. 1.3**

**Zero crossing times of a sinusoid with superimposed noise**

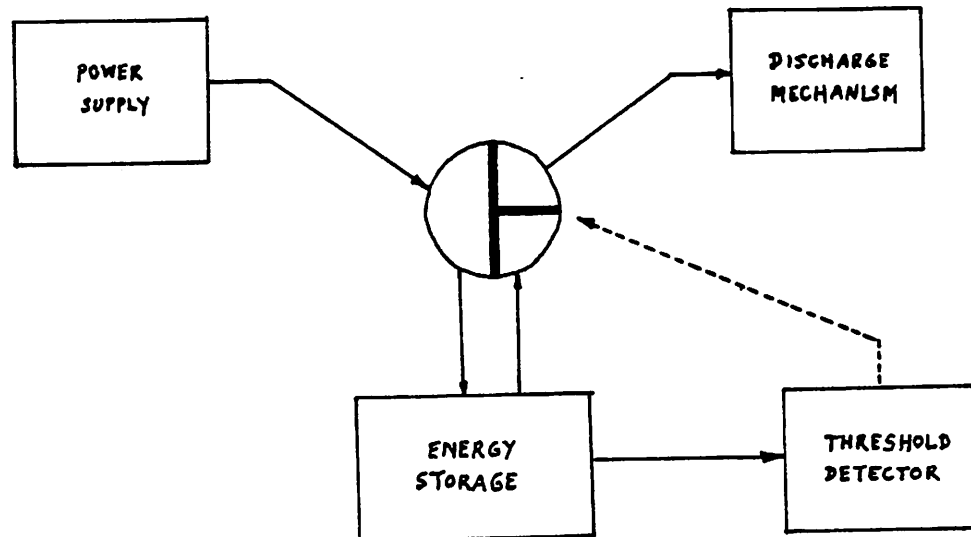


**Fig. 1.4**

**Block diagram of a relaxation oscillator**

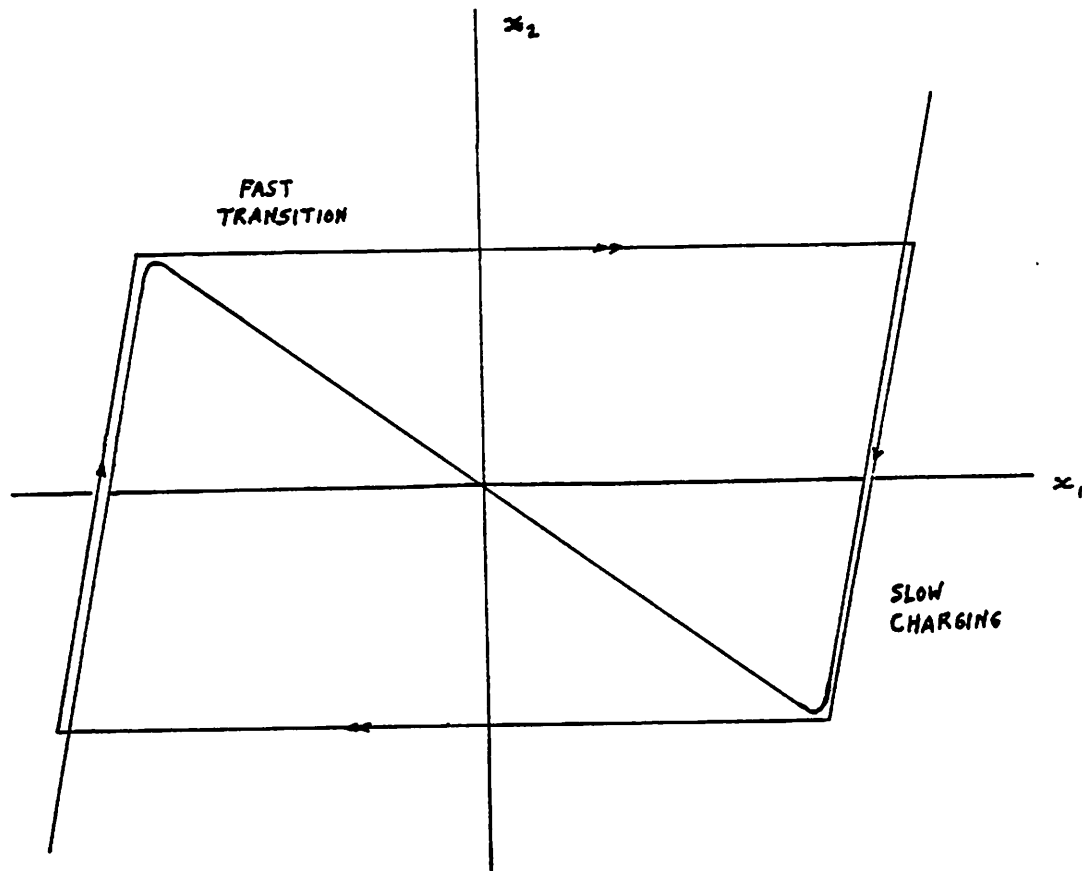


Fig. 1.5

Phase plane trajectory of a relaxation oscillation

Oscilloscope time bases are relaxation oscillators which produce a sawtooth waveform; other, special purpose waveforms can also be produced using suitable charging and shaping schemes. For most timing applications, a symmetrical waveform like a triangle wave and a square wave are desired. Two topologies of oscillator have evolved for such applications, known as the *Grounded Capacitor Oscillator*<sup>3</sup> (G.C.O.) and the *Emitter Coupled Oscillator*<sup>4</sup> (E.C.O.) whose bipolar circuit implementations are shown in Fig.1.6 and Fig.1.7 respectively. The associated waveforms explain their operation. In the G.C.O., the capacitor is alternately charged and discharged by a current between the two thresholds at the input to the Schmitt trigger, whose output then controls the bidirectional current switch. In the E.C.O. the switching and charging-discharging functions are combined. One of the transistors is OFF during one half of the cycle, and when the capacitor voltage reaches a threshold determined by the circuit, this transistor turns ON and the circuit switches to the symmetrically opposite state to continue the other half cycle.

A few general remarks are in order concerning the operation of these circuits. While the capacitor is being charged, the circuit is in one of its astable states, and a fast transition between these states is made regeneratively at certain thresholds. The regenerative aspect is fundamental because of the memory necessary to remember each astable state. The way that the circuit enters its regenerative mode must be understood in detail to see how external disturbances manifest their effect. This is the topic of CHAPTER 3. The waveform at the output of the regenerative portion of the circuit is a square wave.

Unlike harmonic oscillators, there are no frequency selective tuning elements in these circuits. The frequency of oscillation is determined by the *global circuit variables* that is, by the regenerative thresholds of the active circuit, the magnitude of the timing capacitor, and the charging current sources for the topologies of Fig. 1.6 and Fig. 1.7. In particular for the G.C.O., if the Schmitt thresholds are  $V_{t_1}$  and  $V_{t_2}$ , then

<sup>3</sup> A natural outcome of the hysteretic Schmitt trigger [13] <sup>4</sup> Due to Grebene [14]

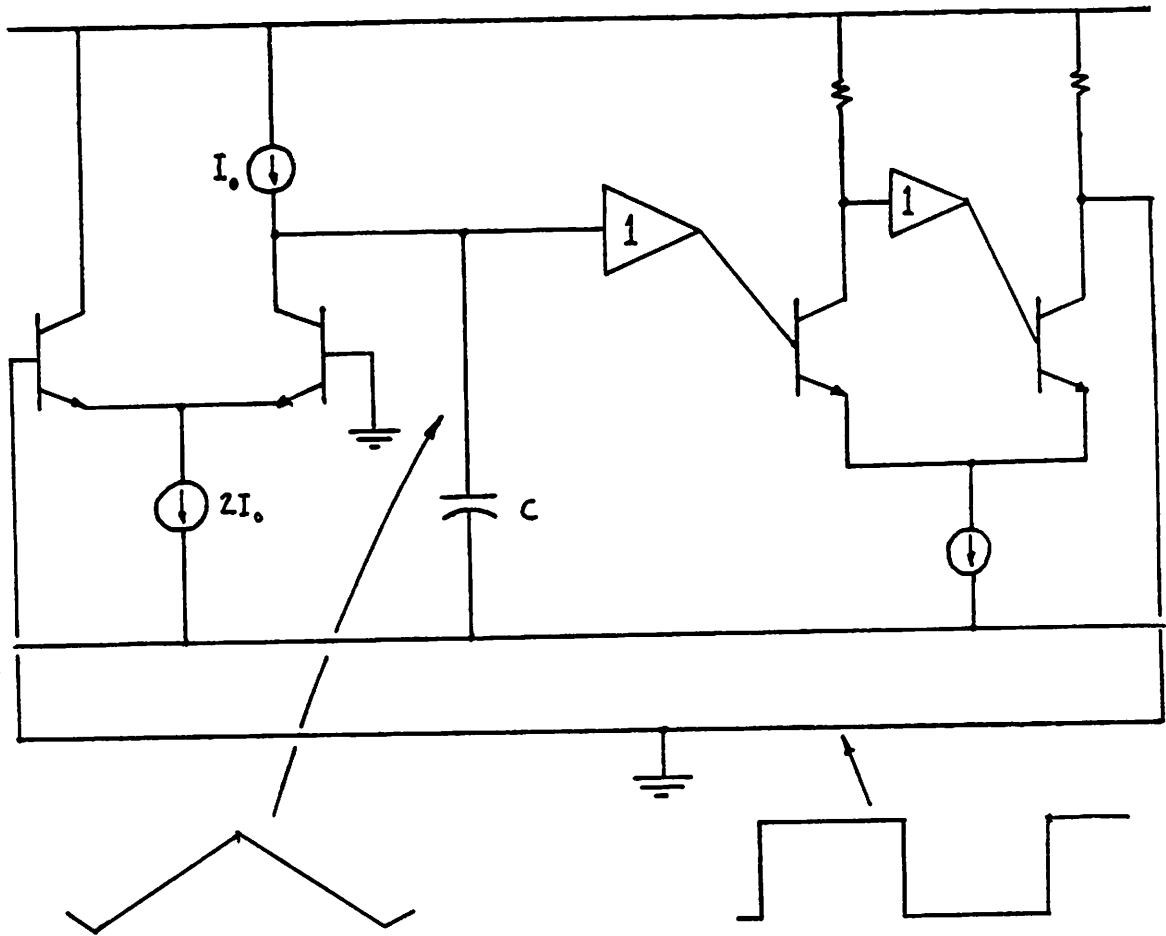
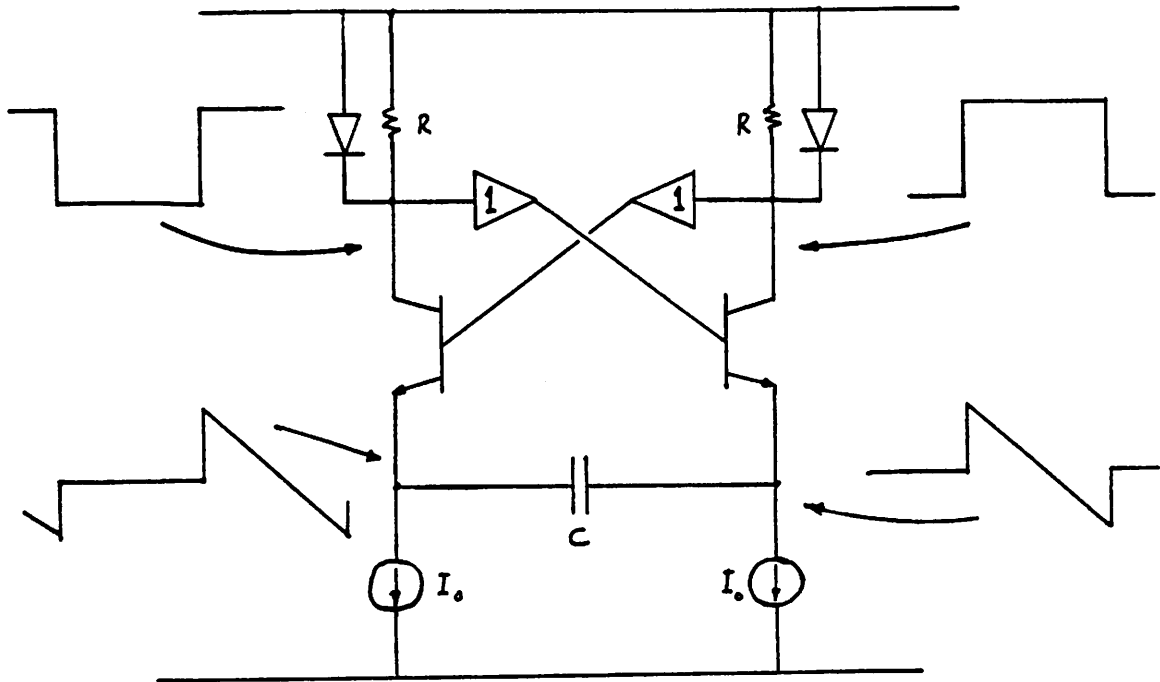


Fig. 1.6

The Grounded Capacitor Oscillator



**Fig. 1.7**  
**The Emitter Coupled Oscillator**

$$f_{osc} = \frac{I_0}{2C(V_{t_1} - V_{t_2})} \quad (1.7)$$

The frequency can be varied with  $I_0$  and, in practice, about four decades of frequency can be swept. More important, the dependence of  $f_{osc}$  on the current is linear, which is necessary for accurate frequency demodulation when the oscillator is used in a Phase Locked Loop. This dependence of frequency on the circuit variables has its disadvantages as well, because the latter can be subject to large drifts due to temperature and other environmental fluctuations. By proper circuit design [3], it is possible to compensate for most of these drifts.

The final limitation of relaxation oscillators, if not the most serious one, is their susceptibility to noise. They are very broadband circuits because they have no embedded frequency selective elements, and thus are subject to noise throughout the frequency spectrum. Noise modulates the switching instants between the astable states, resulting in a *random pulse duration modulated* output square wave. In a frequency demodulator, such a noisy oscillator limits the minimum modulation that can be resolved. Most commercially available relaxation oscillators are inadequate for broadcast quality F.M. demodulation.

---

## CHAPTER 2

---

### Noise in Relaxation Oscillators: Characterisation and Measurement

A noiseless relaxation oscillator produces a perfectly repetitive square wave. Noise randomly modulates this square wave, as shown in Fig. 2.1. The modulation is due to the superimposed noise on the switching current,  $i_0$ , as it approaches a regeneration threshold,  $I_r$ . Regeneration requires the presence of a positive feedback loop, which will also amplify any small-signal noise generator,  $i_n$ , in the circuit as

$$\frac{i_0}{i_n} = \frac{a}{1 - ab} \quad (2.1)$$

where  $ab$  is a function of  $i_0$ , and  $|ab| = 1$  at  $i_0 = I_r$ . At this current, one of the closed loop poles enters the right half plane, and, simultaneously, the small-signal gain becomes infinite. Thus, the noise is subject to a level-dependent gain, and is represented in Fig. 2.2 as a growing noise added to the switching current. If the circuit switches when the noisy current *first crosses the regeneration threshold* there will be an uncertainty in switching instant determined by the root-mean-square (r.m.s.) noise. This model of switching is examined in detail in CHAPTER 3.

The spectrum of a square wave contains an infinite number of harmonics, specified by the following Fourier series:

$$v(t) = \sum_{k=1}^{\infty} \frac{V_0}{k} \sin(2\pi k f_0 t) \quad k \text{ odd} \quad (2.2)$$

where  $f_0$  is the frequency of oscillation. Jitter in the square wave produces sidebands around each harmonic, where the height of each sideband, and thus the power contained in them, varies with the amount of noise. The measured spectrum of a noisy square wave is shown in

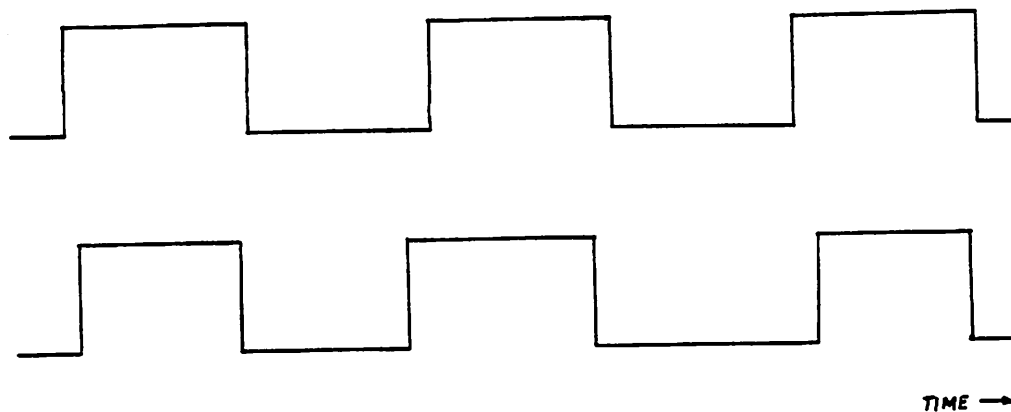


**Fig. 2.1**

**A perfectly repetitive square wave compared to one  
modulated by noise**

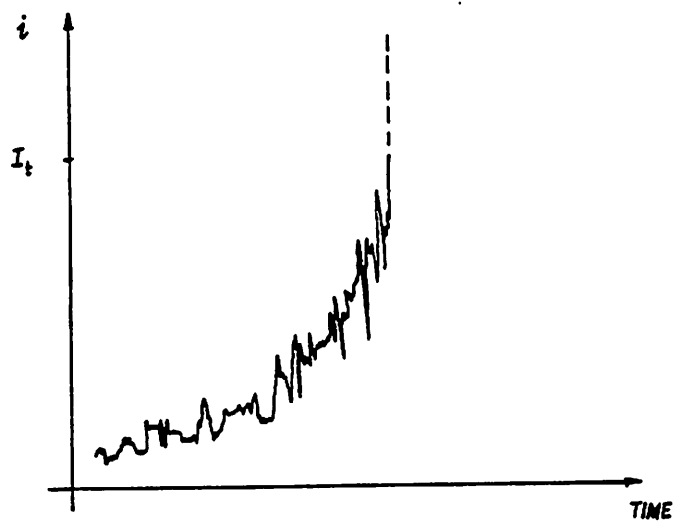


**Fig. 2.2**

**A noisy current waveform in a regenerative circuit**

Figs.2.3(a) and (b). Their shape resembles the noise sidebands for a harmonic oscillator, yet are not produced by a linear filtering action as was the case there. These sidebands can be understood better by considering the spectrum of a single frequency,  $f_1$ , modulating a square wave. From standard f.m. theory [15], this is given by:

$$v_t = \frac{M}{2} \cos(\omega_1 t) + \sum_{k=1}^{\infty} \frac{\sin k\omega_0 t}{k\pi} - \sum_{k=1}^{\infty} \frac{J_0(k\pi M)}{k\pi} \sin(k\omega_0 t - 2k\pi N) - \sum_{k=1}^{\infty} \sum_{l=\pm 1}^{\pm \infty} \frac{J_l(k\pi M)}{m\pi} \sin(k\omega_0 t + l\omega_1 t - 2k\pi N - l\pi/2) \quad (2.3)$$

and is graphically shown in Fig.2.4. An infinite number of side frequencies are produced around each harmonic, and their amplitude envelope is the Bessel function of order  $n$ ,  $J_n$ . When white noise is the modulating signal the discrete side frequencies change into continuous sidebands, but preserve the decaying envelopes as above. So the shape of the sidebands is an *outcome of the modulation process* and not due to a narrowband frequency selection.

Alternatively, the phase jitter can be represented in the *time domain* as the standard deviation of single pulse periods. When defined this way, it becomes more tedious to measure the jitter because a large number of single cycle periods must be obtained to generate a reliable histogram. Recently available instruments<sup>5</sup> can automatically produce the desired statistics, thus making this definition a feasible one in practice.

There is no standard way of specifying phase jitter in square waves: technical journals or manufacturers' specification sheets seem to exercise the choice between the frequency and time domains quite arbitrarily. Before proposing a standard definition, let us consider how noise affects the oscillations. Noise in a harmonic oscillator modulates the phase continuously, and thus produces a random "distortion" in a sine wave; whereas, in a relaxation oscillator, it varies the instants of transition between the two astable states. Thus, it is appropriate to specify phase noise in a sine wave in the frequency domain, and the phase jitter in a square wave in the time

<sup>5</sup> Like the HP 5370 microprocessor controlled frequency counter.

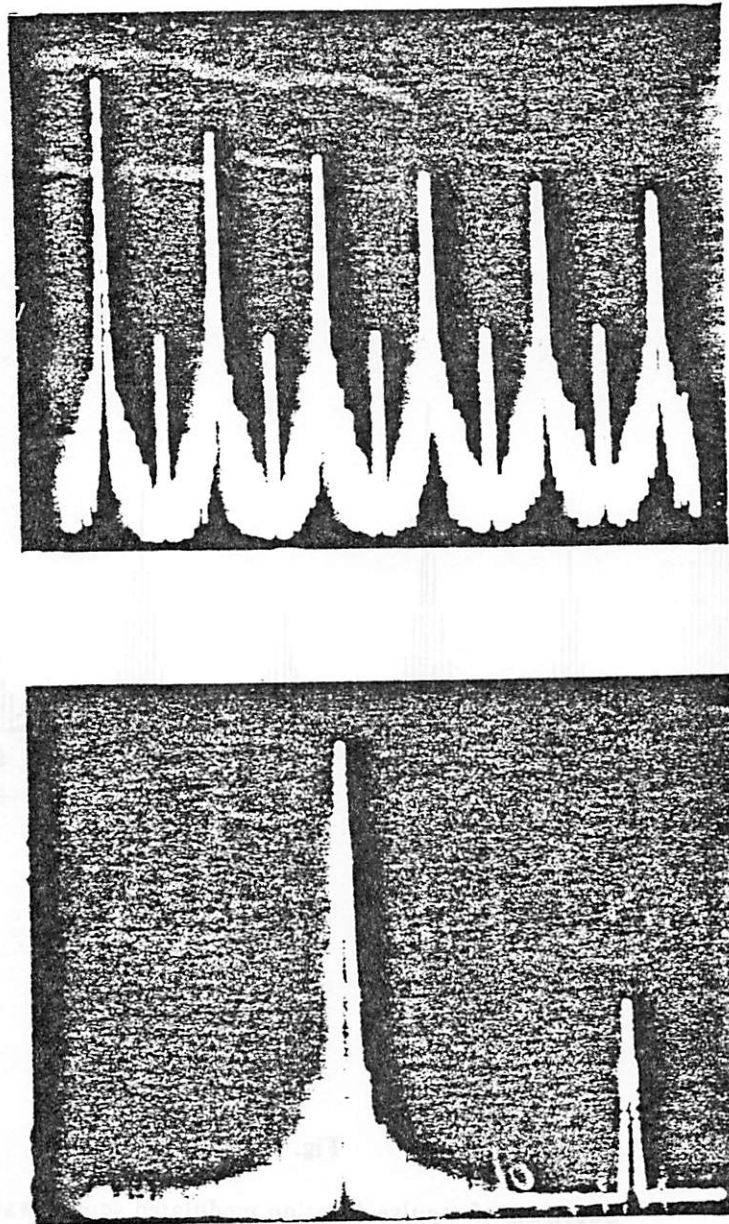


Fig. 2.3

Measured spectra of square waves with jitter

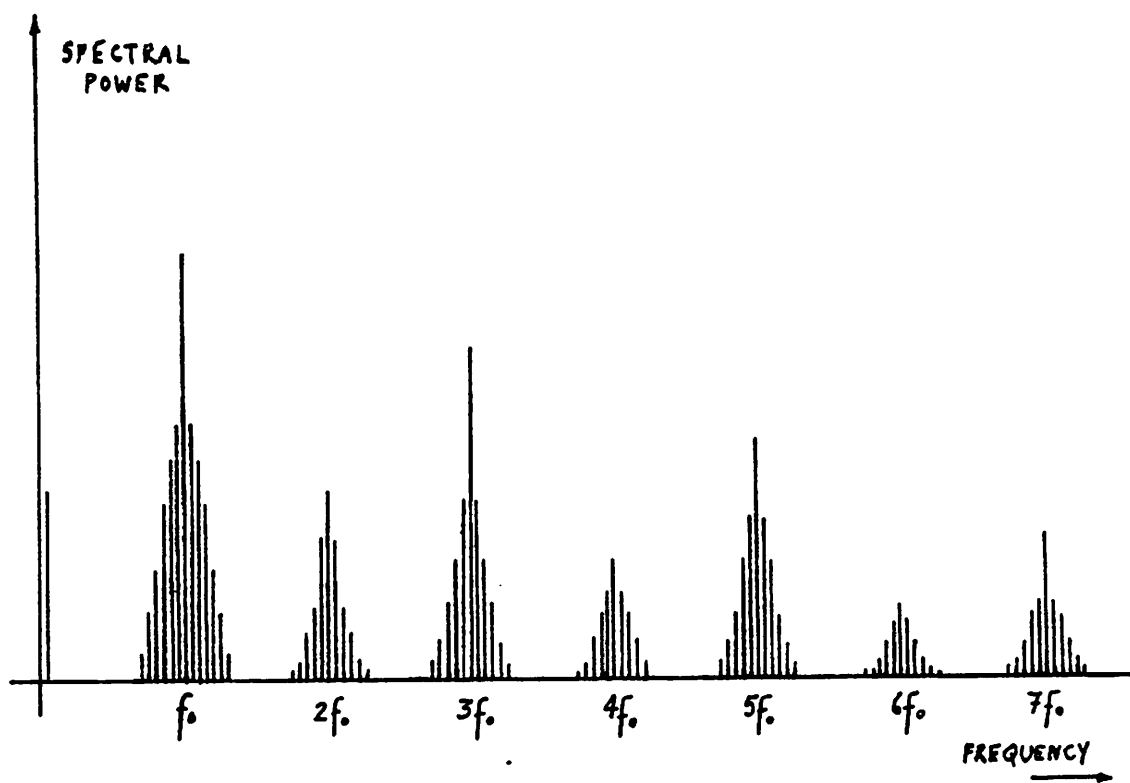


Fig. 2.4

Spectrum of a pulse duration modulated square wave,  
single modulating frequency

domain. In this study, the following definition is used:

$$JITTER = \frac{STANDARD\ DEVIATION\ OF\ SINGLE\ CYCLE\ PERIODS}{AVERAGE\ PERIOD}$$

This normalised quantity is specified in parts per million (p.p.m.) of the oscillation period.

An oscilloscope can be used as a rough and ready method to measure phase jitter without having to plot a histogram. This method is fairly accurate, particularly if a dual time-base oscilloscope is used when measuring small jitter. The procedure is as follows: One complete cycle of oscillation is displayed on the main time base, and its transition edge is magnified in time using the delayed time base. Any jitter produces a "fuzz" in this edge; an example of this is shown in Fig. 2.5. The maximum thickness of the fuzz is about 4 times its standard deviation. The factor of 4 is due to the statistics of the process, discussed later. This measurement is prone to error in two ways: first, the measured fuzz can change substantially with the brightness of the oscilloscope trace, and second, improper triggering of the time base gives too large a value of measured jitter. However, exercising precaution by using the maximum brightness available before the trace distorted, and by adjusting the triggering levels to minimise the fuzz, we obtained results which corresponded well with more accurate measurements. Finally, the oscilloscope time base itself adds a negligible jitter to the measured value, as discussed in CHAPTER 3.

Let us examine the jitter performance of some widely used voltage-controlled oscillator (V.C.O.) circuits, all of which work on the relaxation principle. Standard operating conditions have to be used to compare their performance, and these were decided to be  $f_{osc} = 1$  kHz and the capacitor charging current = 1mA. The results of the measurements are shown in Table 1. The AD 537 is the lowest jitter V.C.O. available commercially. To put these numbers in perspective, we examine the jitter requirements for broadcast quality f.m. demodulation assuming that a Phase Locked Loop (P.L.L.) demodulator is used. The following specifications apply: Intermediate frequency (i.f.) = 10.7 MHz; maximum deviation of carrier = 200 kHz; maximum modulating frequency = 15 kHz; and, the dynamic range of modulating signal = 80 dB.

V.C.O.	Topology	Cycle-to-cycle jitter at 1kHz.
Signetics NE 562	G.C.O.	125 p.p.m.
Signetics NE 565	E.C.O.	250 p.p.m.
Wavetek 132 (function generator)	G.C.O.	70 p.p.m.
Analog Devices AD 537	E.C.O.	25 p.p.m.

Table 1

Measured jitter at 1 kHz of standard V.C.O.s

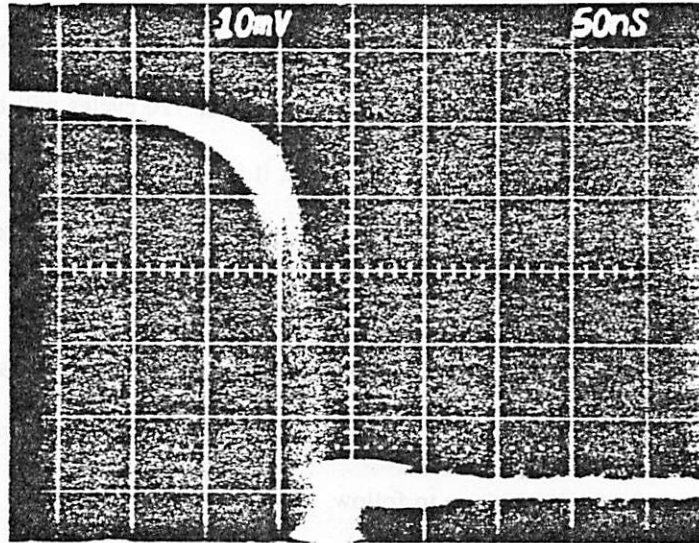


Fig. 2.5

Oscillogram of a single cycle transition of  
a jittered square wave

Therefore, the minimum deviation of the carrier is  $-80$  dB of  $200$  kHz  $= 20$  Hz. If the demodulator operates at the i.f., it should ideally be able to resolve a shift of  $20$  Hz in  $10.7$  MHz, i.e.  $2$  p.p.m.; however, its resolution shall be limited by the cycle-to-cycle jitter in the local relaxation oscillator. What is the maximum tolerable jitter in the oscillator to will meet this requirement? If all the modulating power was concentrated at  $15$  kHz, then  $10.7 \times 10^6 / 15 \times 10^3 = 720$  cycles will elapse per cycle of information. So if the V.C.O., nominally oscillating at  $10.7$  MHz, has  $N$  p.p.m. jitter per cycle, the jitter in ensembles of  $720$  cycles will be  $N/\sqrt{720}$ <sup>1</sup>. For the jitter to be less than the minimum modulation, it is required that  $N/\sqrt{720} = 2$  p.p.m., i.e.  $N=53$  p.p.m. Strictly speaking, this is the bound on the "peak-to-peak" jitter, so the r.m.s. jitter bound should be  $1/4$  of this, i.e. less than  $14$  p.p.m.

None of the V.C.O.s in Table 1 meet this requirement, and Phase Locked Loops are consequently not used as f.m. demodulators [16]. The  $14$  p.p.m. can be regarded as the value to be attained in the circuit designs to follow.

<sup>1</sup> After frequency division, or period multiplication, the jitter of a divided square wave of period  $NT$  is less than that of the original signal of period  $T$  by a factor of  $1/\sqrt{N}$ . Each cycle of the divided frequency corresponds to  $N$  cycles of the original frequency, and by the Central Limit Theorem [17], if the standard deviation of each cycle of the latter is  $\delta T$ , then that of the divided frequency is  $\sqrt{N}T$ . The fractional Jitter, however, is this uncertainty divided by the period, and so  $1/\sqrt{N}$  times reduced.

---



---

## C H A P T E R 3

---

### A Theory of Jitter in Relaxation Oscillators

To motivate the following discussion, the Emitter Coupled Oscillator (E.C.O.) is considered in detail, and the results are generalised to other circuits at the end of the chapter. The circuit discussed is shown in Fig. 3.1, marked with the necessary circuit variables. We assume that all the noise sources in the circuit can be lumped into the single noise current source,  $i_n$ , and that the rest of the circuit is noiseless; that this assumption is valid for every noise source other than the timing current sources shall become evident. The unity gain elements are assumed to be perfect buffers. We consider the circuit dynamics when transistor Q1 is turning ON, and carries a small current  $i < I_1$ , so the differential equations describing the circuit are:

$$\dot{v}_{e_2} - \dot{v}_{e_1} = \frac{I_0 - i}{C} \quad (3.1)$$

$$v_{b_2} = v_{c_1} = V_{cc} - (i - i_n)R \quad (3.2a)$$

$$v_{b_1} = v_{c_2} = V_{cc} - (2I_0 - i)R \quad (3.2b)$$

$$v_{be_1} = V_T \log_e \frac{i}{I_s} \quad (3.3a)$$

$$v_{be_2} = V_T \log_e \frac{2I_0 - i}{I_s} \quad (3.3b)$$

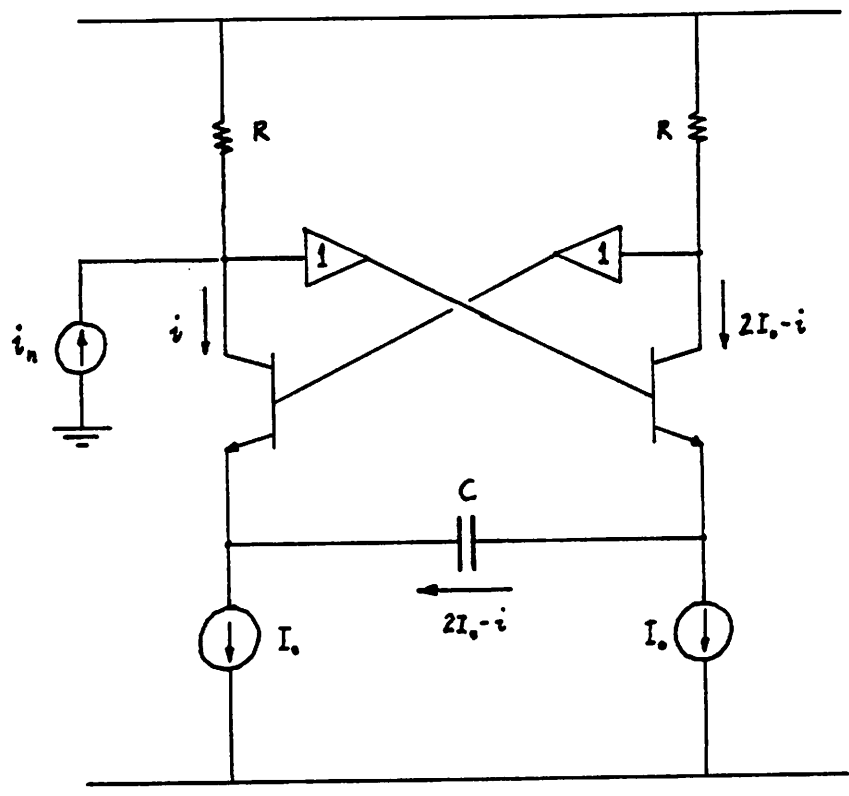


Fig. 3.1

Emitter Coupled Oscillator used for analysis

where  $V_T = kT/q$  (the thermal voltage)

and  $I_s =$  saturation current of B-E junction.

Upon eliminating the transistor voltage variables from these equations we get:

$$\frac{di}{dt} = \frac{\frac{I_0 - i}{C} + R \frac{di_n}{dt}}{\frac{V_T}{i} - R} \quad (3.4)$$

Rather than solving (3.4) exactly, let us examine its solutions qualitatively. We can do so by plotting the vector field generated by the R.H.S. of (3.4) in the  $i-t$  plane, and studying the trajectories resulting from this vector field. In the absence of noise, the trajectory of Fig. 3.2(a) is obtained; note that its slope becomes infinite at the threshold of regeneration  $I_r = \frac{V_T}{R}$ , when the denominator of the R.H.S. of (3.4) becomes zero. For  $i > I_r$ , this differential equation no longer describes the circuit because the dynamics of the circuit are then determined by the various parasitic capacitors at its nodes.

Another differential equation applies for this part of the oscillation because, by ignoring the parasitic components, (3.4) is an incomplete description of the circuit. The order of the set of differential equations describing the circuit would increase by one for each independent parasitic energy storage that was included, so that for  $n$  parasitic capacitors  $C_{\epsilon_1}, \dots, C_{\epsilon_n}$  and the timing capacitor  $C$ , the differential equations would be

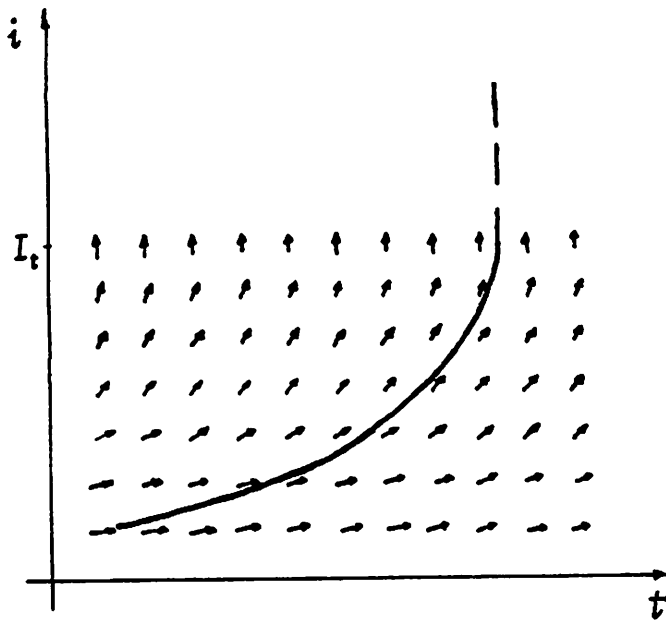


Fig. 3.2(a)

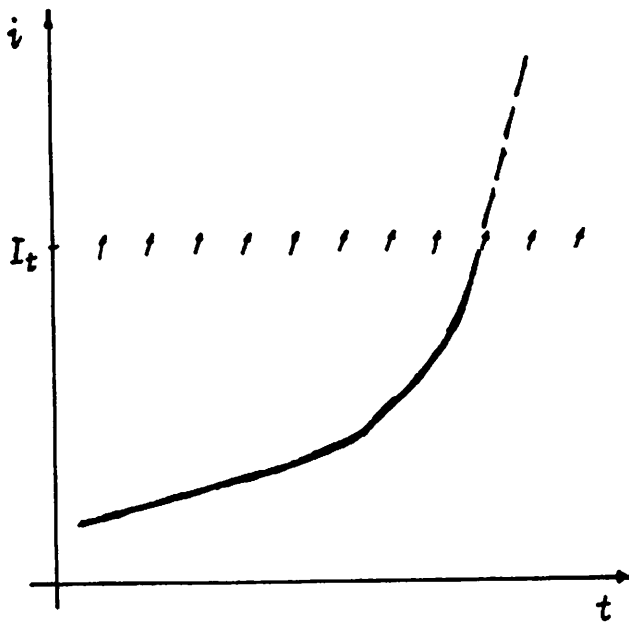


Fig. 3.2(b)

Switching trajectories of oscillator without,  
and with, parasitic capacitances

$$C \dot{v}_0 = f_0(v, v_1, \dots, v_n) + i_n$$

$$C_{\epsilon_1} \dot{v}_1 = f_1(v, v_1, \dots, v_n)$$

(3.5)

$$C_{\epsilon_n} \dot{v}_n = f_n(v, v_1, \dots, v_n)$$

The circuit must be decomposed systematically and exhaustively into an n-port for such a description [18], but often, guided by intuition, only a few important parasitics need to be considered.

When a complete description of the system is used the slope of the switching current<sup>6</sup> never becomes infinite, but rather is limited to a finite slew rate by the parasitics<sup>7</sup>, as in Fig. 3.2(b). However, as the parasitics are much smaller than the timing capacitor, the dynamics can be separated into a *slow time scale* during relaxation, and a *fast time scale* during regeneration, the transition between the two being made smoothly in the approach to regeneration, when the circuit becomes a *variable gain amplifier*. The difference between these two time scales is typically large enough that we can adequately describe the effects of noise using the simplified model of (3.4).

As the circuit approaches regeneration, the "signal" and noise components of  $di/dt$  grow at an equal rate because they have a common denominator which approaches zero. While  $0 < i < I_t$ , the circuit is being *driven by the capacitor ramp voltage*, the first term on the R.H.S. of (3.4); the relaxation period, where Q1 is OFF and  $i \approx 0$ , is included in this regime. For  $I_t < i < 2I_0$  the circuit enters an *autonomous switching regime*, where the dynamics are independent of the driving ramp. These two portions of the switching transient are summarised

<sup>6</sup> We refer to a switching *current* for the example being considered, whereas in general it will be a suitable set of state variables [18].

<sup>7</sup> For an incremental description of the system in the s-plane, this corresponds to some pole attaining a finite value in the right-half plane.

in Fig. 3.3.

The noise term in the numerator of (3.4) adds a random component to  $di/dt$  at each point, so that the instant,  $T$ , of crossing the regeneration threshold is modulated, as illustrated in Fig. 3.4. Jitter is the r.m.s. variation in  $T$  produced by a given r.m.s. value of  $i_n$ <sup>8</sup>. We now estimate this variation. Separating variables in (3.4) and integrating from some reference time  $t=0$  (in the relaxation period, where  $i(0)=0$ ) to  $t=T$ , we get

$$\int_0^{I_0 - \frac{V_T}{R}} \left( \frac{V_T}{i} - R \right) di = \int_0^T \frac{I_0 - i}{C} dt + R \int_0^T \frac{di_n}{dt} dt$$

Now  $i \leq I_0 \ll I_0$  for  $0 < t \leq T$ , because  $V_T/R$  is typically only a few microamps while  $I_0$  is milliamps. Furthermore, the L.H.S. of the equation is completely determined by circuit variables and is independent of the random variables  $i_n$  and  $T$ . So,

$$K \text{ (a constant)} = \frac{I_0 T}{C} + R i_n(T)$$

We are interested in the variations in  $T$  due to  $i_n$ . This equation shows that the sum of two random variables on the R.H.S. equals a constant, so the variations in  $i_n$  must be balanced by variations in  $T$ . Re-writing the equation as

$$K - \frac{I_0 T}{C} = R i_n(T) \quad (3.6)$$

it can be graphically solved, as in Fig. 3.5, where the circuit is assumed to switch when the ramp first crosses a noisy threshold.  $T$  will vary slightly each time the circuit switches, and

$$\text{Variation in } T \leq \frac{\text{Variation in threshold value}}{\text{Slope of ramp}} \quad (3.7)$$

so that, in terms of standard statistical notions, if  $\sigma(\cdot)$  is the standard deviation, then<sup>9</sup>

<sup>8</sup>The noise may have any statistical distribution.

<sup>9</sup>This inequality requires proof, which is given in CHAPTER 4.

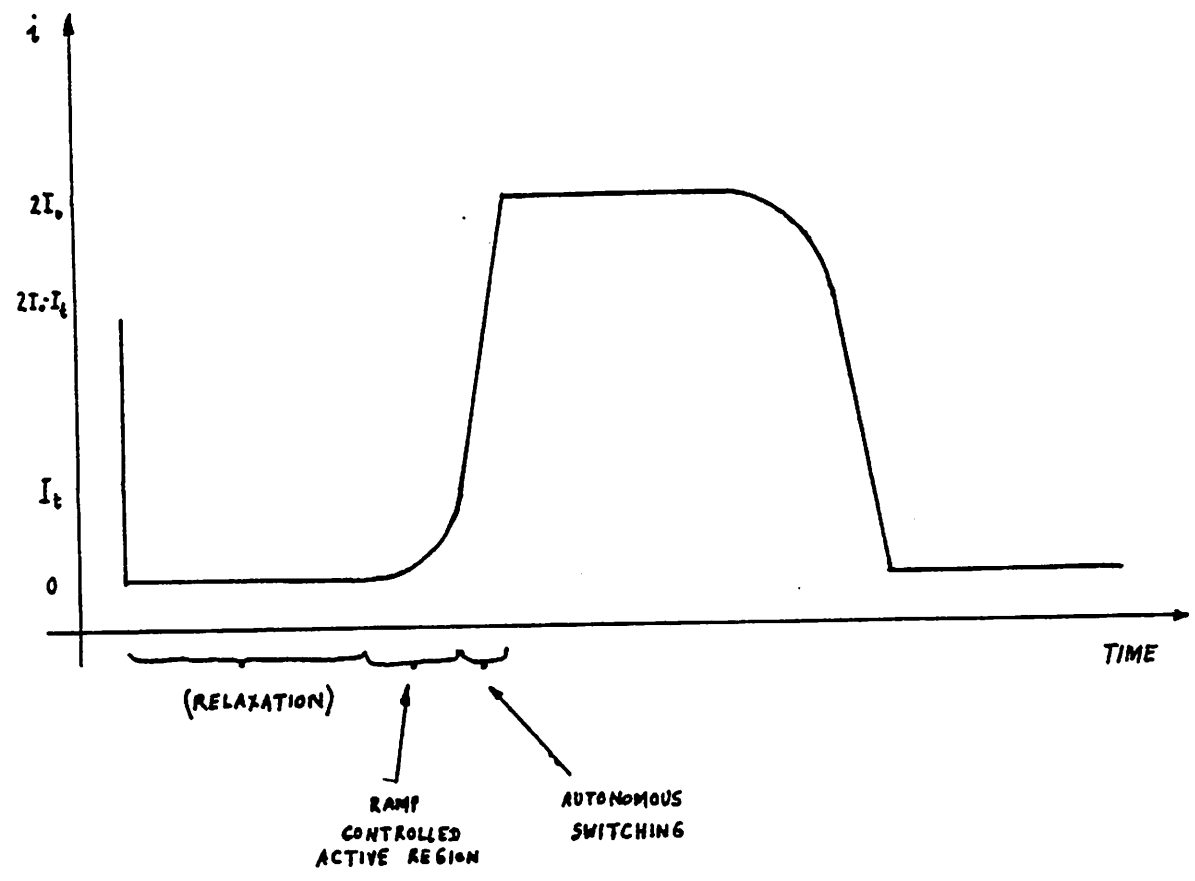


**Fig. 3.3**  
**The two regimes of the switching process,**  
**while the circuit is active**

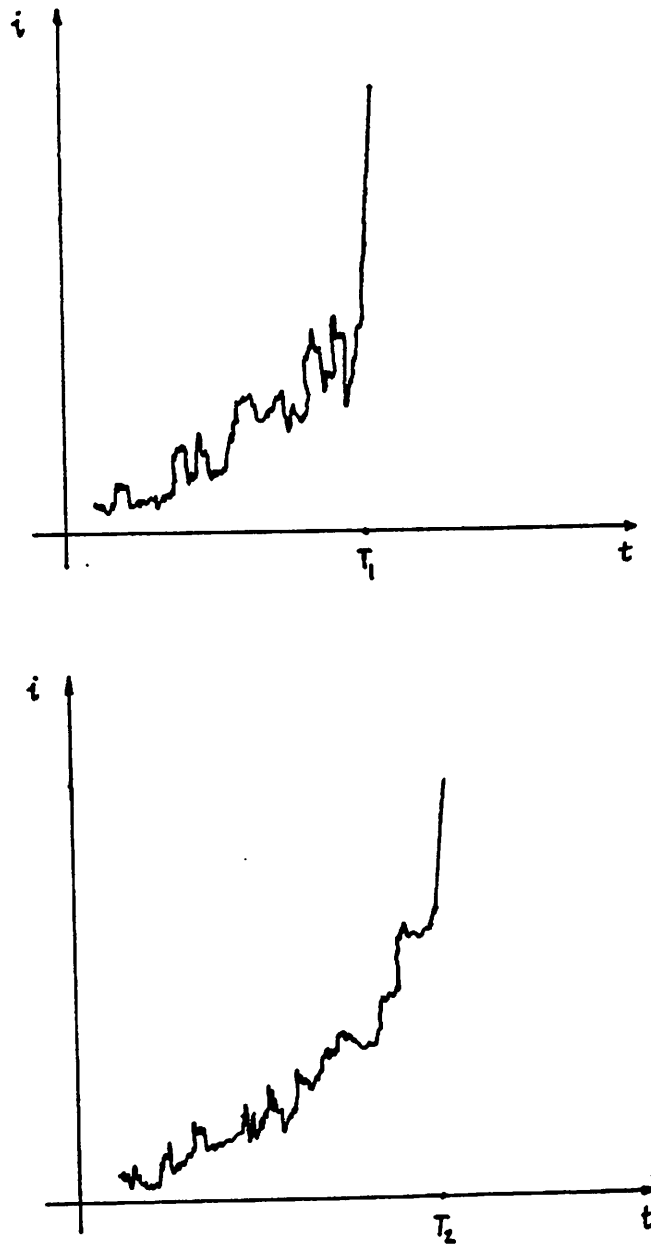


**Fig. 3.4**  
**Modulation of the regeneration instant,  $T$ ,**  
**by superimposed noise**

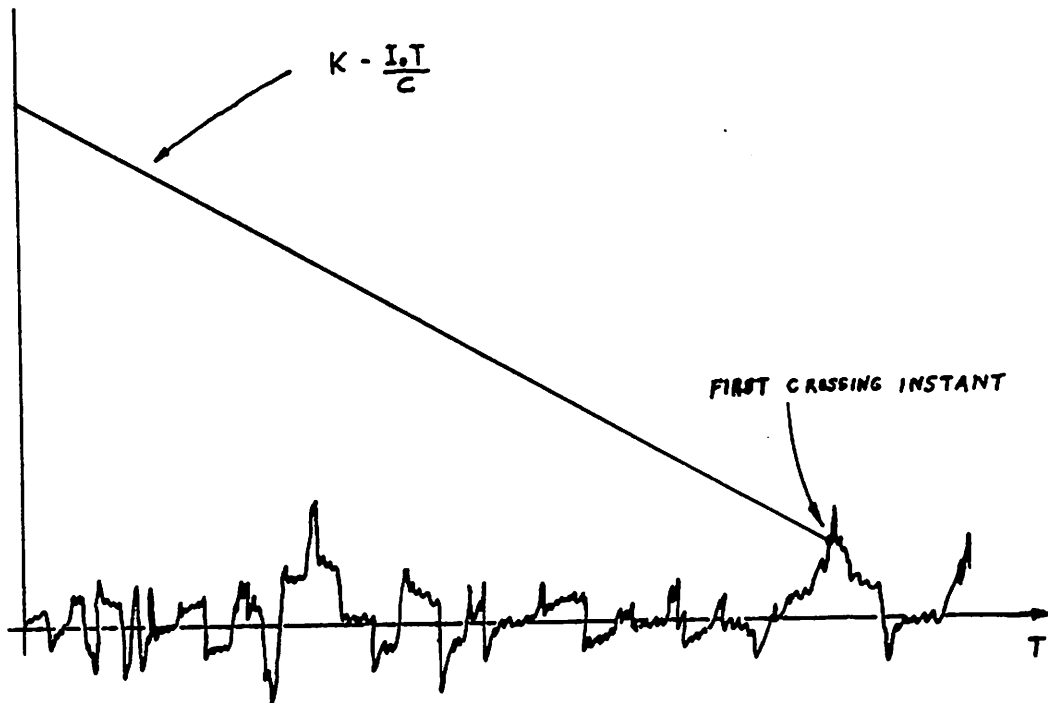


**Fig. 3.5**

**Graphical solution of the noisy switching equation**

$$\sigma(T) \leq \frac{RC}{I_0} \sigma(i_n) \quad (3.8)$$

Thus, we have an upper bound on the jitter per switching.

The ramp crossing the noisy threshold is the main model of jitter production to be used in the rest of this study. The following question arises concerning the results of the analysis thus far: How is it that a linear ramp represents the switching of a non-linear circuit? The answer lies in the fact that in Fig. 3.5 the horizontal axis is *not* real time,  $t$ , but rather the regeneration instant,  $T$  (measured with respect to some suitable origin  $T=0$ ). The dynamics of the circuit in time  $t$  will still resemble Fig.3.2(a), but their (non-linear) details are unimportant if we are only concerned with the variations in  $T$ . Alternatively, we can think of Fig. 3.5 as being obtained by a smooth deformation of the time scale of Fig. 3.2(a), and because the signal and noise currents grow at the same rate, they are linearised with respect to each other. It is important to note that this linearisation is not due to an incremental model of the circuit, but is the outcome of a large-scale analysis.

The above results are independent of the statistics of the noise. If the noise satisfies a Gaussian distribution, as is normally the case, what are the statistics of the first-crossing times? They are clearly not Gaussian for broadband white noise because the first-crossings shall mostly occur at the positive peaks of the noise waveform, and almost always before the ramp reaches its mean value. Therefore, a peculiar distribution of  $T$  will result. This *First Crossing Problem* [19],[20] was motivated originally in the 1940s by attempts to reduce the noise sensitivity of pulse triggered circuits, but remains unsolved; consequently, there is no analytic form for the statistics. We have, nevertheless, obtained some quite useful empirical results to this end, detailed in CHAPTER 4.

What if the disturbing signal,  $i_n(t)$ , is not random, but rather is periodic? If it is near a multiple or sub-multiple of the oscillator frequency, it will try to *synchronise* the oscillation to its own frequency under certain conditions. This is an extremely interesting and detailed study in its own right, and has occupied a central role in recent dynamical system theory[21]. Suffice

it to say that the model developed here gives an insight into how a periodic signal would exert its influence on the oscillator from cycle to cycle during the short period of time while the circuit approaches regeneration.

Even though it is an upper bound, the result (3.8) is useful because it specifies the variables which can be used to reduce the jitter. Strictly speaking, the jitter is the uncertainty in  $T$  normalised to the period, so that if the triangle wave is  $V_\Delta$  volts peak to peak, then

$$Jitter \sim \frac{\sigma(T)}{2V_\Delta \frac{C}{I_0}} < \frac{R\sigma(i_n)}{2V_\Delta} \quad (3.9)$$

The numerator of the last term is the r.m.s. noise voltage at the collector of the E.C.O., which, by the follower action of the circuit, appears in series with the timing capacitor. It is always possible to refer all the small signal noise voltages and currents in the circuit to an *equivalent source*  $v_n$  in series with the timing capacitor, while the circuit is near regeneration. Noise in the current sources  $I_0$ , for example, will be converted into a voltage at the collector after passing through Q2 (Fig. 3.1), so then

$$Jitter = \frac{v_n}{2V_\Delta} \quad (3.9)$$

What is the jitter due to a noise current  $i_{n_c}$  through  $C$ ? The following differential equation describes the circuit if this were the only source of noise:

$$\frac{di}{dt} = \frac{\frac{I_0 - i}{C} + \frac{i_{n_c}}{C}}{\frac{V_T}{i} - R} \quad (3.10)$$

Using the same procedure as before to integrate it, we get

$$\int_0^T \left( \frac{V_T}{i} - R \right) di = \frac{I_0 t}{C} + \frac{1}{C} \int_0^T i_n(t) dt$$

so that

$$\sigma(T) \leq \frac{1}{I_0} \sigma \left\{ \int_0^T i_{n_c}(t) dt \right\} \quad (3.11)$$

The capacitor integrates the noise current, and the variance of the resulting voltage determines  $\sigma(T)$ . An analytic expression is derived in Appendix 1 for this variance, assuming that  $i_{n_c}$  is white noise with density  $\hat{i}$  A/ $\sqrt{\text{Hz}}$ , whence

$$\sigma(T) \leq \frac{\hat{i}}{I_0} \sqrt{T} \quad (3.12)$$

This completes the characterisation of all the noise sources.

Appendix 2 extends these results to an E.C.O. consisting of generalised active devices and non-linear loads.

The analysis can easily be extended to the G.C.O. topology. Here, the regenerative element is the Schmitt trigger, which is analysed exactly as above, except that the capacitor is outside the loop. The results of the analysis are identical to (3.9) and (3.12) above, which is not surprising because the two circuits are duals of one another, their apparent differences being in no way fundamental. The E.C.O. and G.C.O. are schematically compared in Fig. 3.6 to emphasise their similarities.

For completeness, we consider the case when the magnitude of  $I_t$  becomes comparable to  $I_0$ . The denominator of (3.8) should then be  $(I_0 - I_t)$  because

$$\Delta \left( \int_0^T \frac{I_0 - i}{C} dt \right) = \frac{I_0 - i(T)}{C} \Delta T = \frac{I_0 - I_t}{C} \Delta T$$

for small  $\Delta T$ .

The estimates of uncertainties in switching time apply to a single transition, with the reference time  $T = 0$  being the previous transition. The jitter, however, is defined as the uncertainty in widths of complete cycles. As shown in Fig. 3.7, noise affects a complete cycle

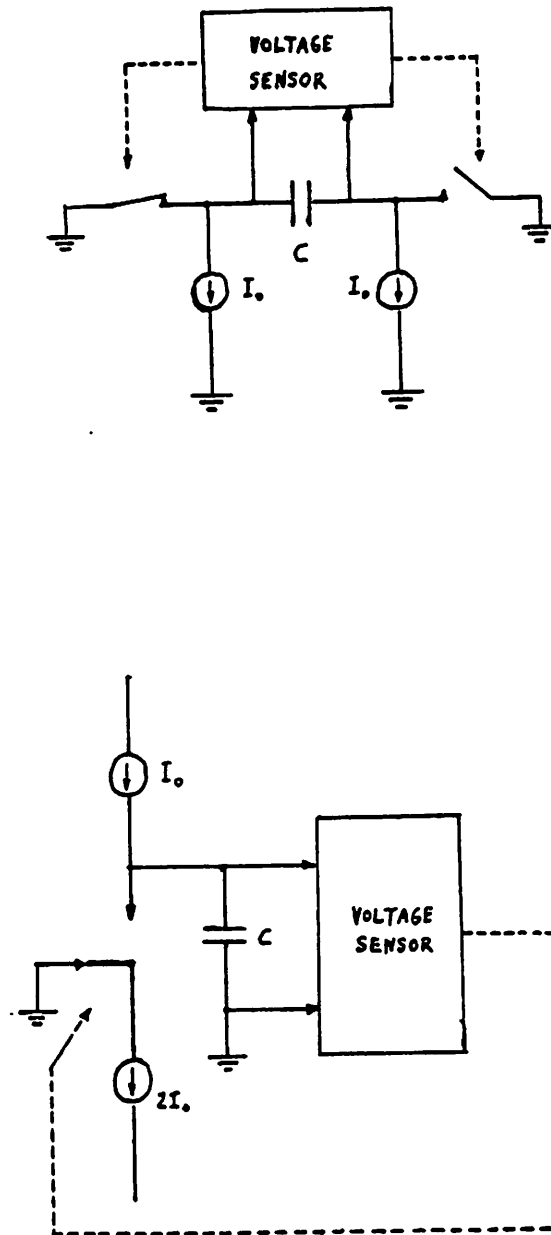


Fig. 3.6

Schematic comparison of the E.C.O. and G.C.O. topologies

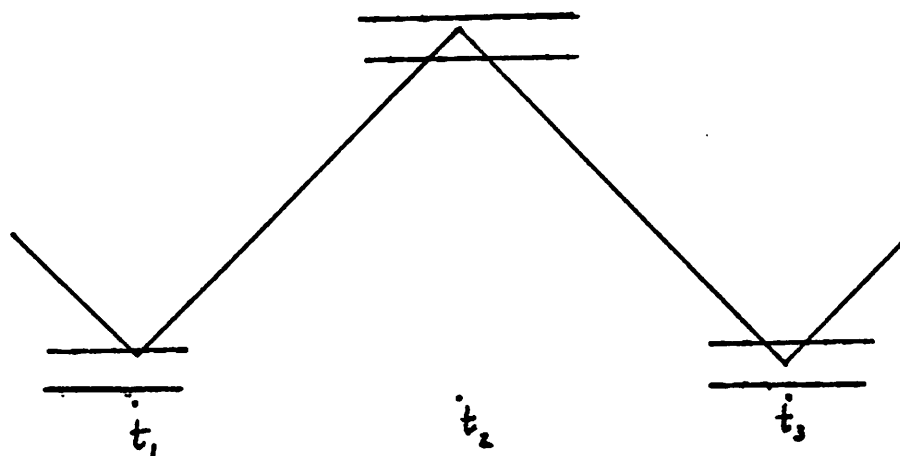


Fig. 3.7

Noise in a complete cycle

at three distinct times: the starting point ( $T_1$ ), the half cycle point ( $T_2$ ) and the end point ( $T_3$ ). The uncertainty at each of these points is  $v_n(T_1)/\lambda$ ,  $2v_n(T_2)/\lambda$ , and  $v_n(T_3)/\lambda$  respectively, where  $\lambda$  is the slope of the ramp, and the uncertainty is doubled at  $T_2$  because noise equally affects both the upgoing and downcoming ramps. If  $v_n(T_1)$ ,  $v_n(T_2)$  and  $v_n(T_3)$  are uncorrelated (which is the case when most of the noise power is contained in higher frequencies than  $f_{osc}$ ), and if they have the same r.m.s. value (which is the case if the oscillator circuit is symmetrical), then

$$\sigma(T) \leq \frac{\sqrt{\sigma(v_n^2(T_1)) + 4\sigma(v_n^2(T_2)) + \sigma(v_n^2(T_3))}}{\lambda} = \sqrt{6} \frac{\sigma(v_n)}{\lambda}$$

This factor of  $\sqrt{6}$  must always be taken into account in making predictions of cycle-to-cycle jitter<sup>10</sup>.

The model of the noisy oscillator is shown in Fig. 3.8, where the capacitor is replaced by an ideal voltage source because it does not exert any integration effect on the noise voltage; equivalently, we can think of the series effect of the capacitor as being inherent in (3.4), the function of the timing capacitor being to provide a ramp voltage. The resulting waveform is a *noisy ramp* which triggers the regenerative element to produce the oscillation. With the noise thus referred back to the undefiled ramp, we have yet another explanation for the linearisation in Fig. 3.5.

### Experimental results

We now have a very simple model for jitter production, consisting of a ramp crossing a noisy threshold. There is an upper bound for the r.m.s. uncertainty in period ( $\delta T$ ) due to the noise in the circuit, given by the ratio of the noise voltage to the ramp slope. From this model, it is evident that the jitter is in fact, directly proportional to this bound. This has been verified experimentally, by obtaining a linear fit in the plots of r.m.s.  $\delta T$  vs. noise (Fig. 3.9), and r.m.s.

<sup>10</sup>Should the triangle wave not be symmetrical, the appropriate  $\lambda$ 's must be taken into account.

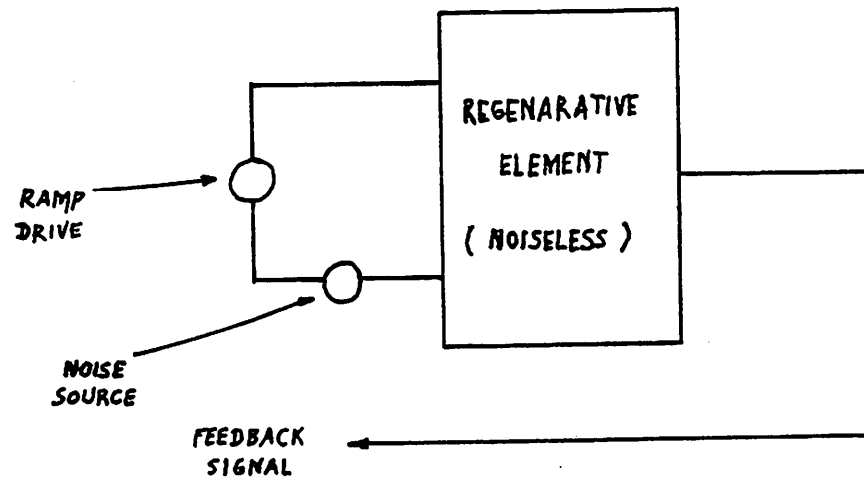


Fig. 3.8

Equivalent input noise model of the relaxation oscillator

---

$\delta T$  vs. ramp slope (Fig. 3.10).

A technique we used throughout this study was to measure the jitter produced in an oscillator due to a known and controllable amount of noise; in particular, this is how the data of Fig. 3.9 was obtained. This was done by injecting a noise current, derived from an external noise source, into an appropriate node of the circuit. The noise signal was chosen to be large enough to dominate the inherent noise in the circuit, but not so large that it grossly altered the circuit's operation. We could then extrapolate the results to estimate the response to the inherent noise.

Injecting an external noise allowed independent control of its amplitude and bandwidth; furthermore, the response at different nodes of the circuit to the same noise signal could be compared, thus establishing their relative sensitivities. Finally, the injected signal could be a periodic one, to investigate the synchronisation properties of the oscillator.

### **Noise bandwidth of relaxation oscillators**

Which elements of a relaxation oscillator determine the bandwidth limitation on white noise in the circuit? With few exceptions, it is the regenerative element which does so, because as it approaches regeneration, at least one of its poles moves towards the origin in the  $s$ -plane and becomes the dominant pole in the circuit. As discussed in CHAPTER 2, the pole movement is a natural consequence of positive feedback. It is either a parasitic or a device capacitance which is responsible for producing this pole, because the timing capacitor's effect is completely specified in (3.2), and clearly it only provides the necessary ramp without any bandlimiting. The solution to this differential equation will admit noise at any frequency whatsoever without attenuation.

To see the high frequency rolloff characteristics, we must solve the complete differential equation, inclusive of parasitics (3.5). We found no convenient way of qualitatively

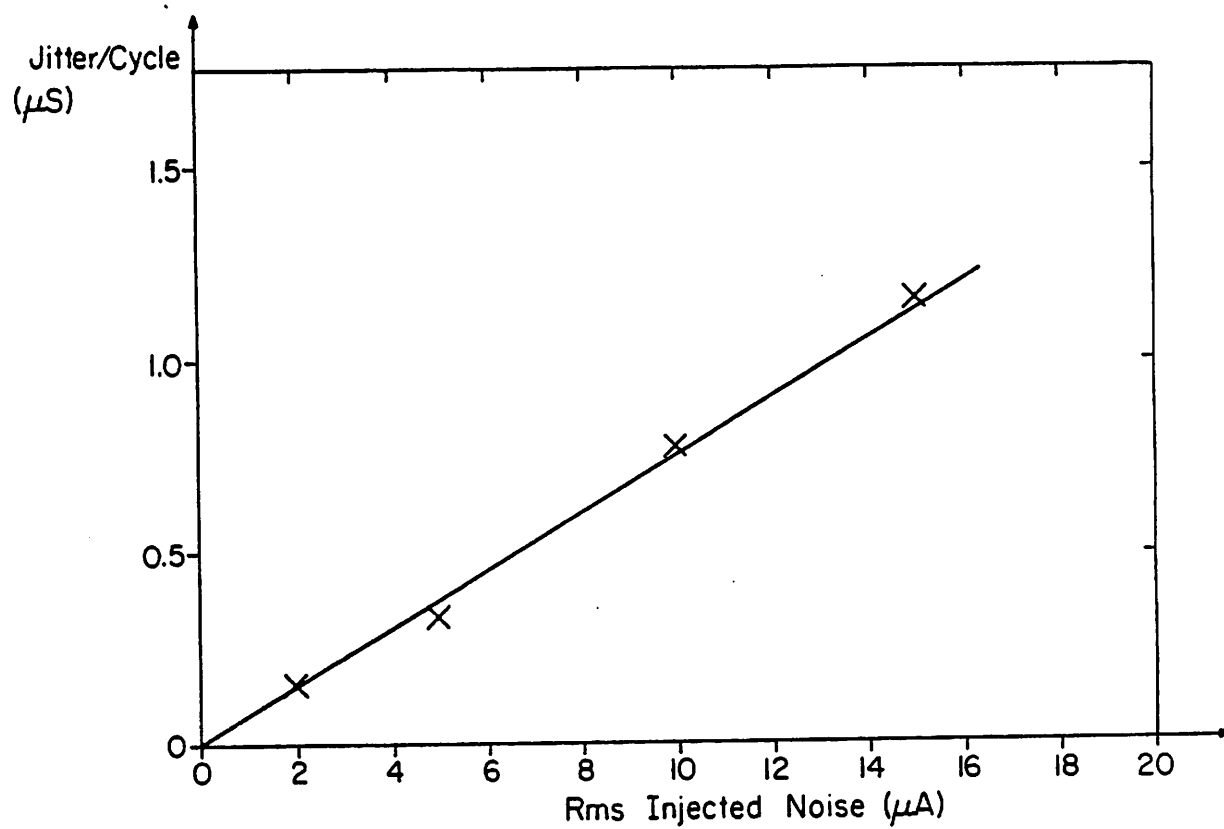
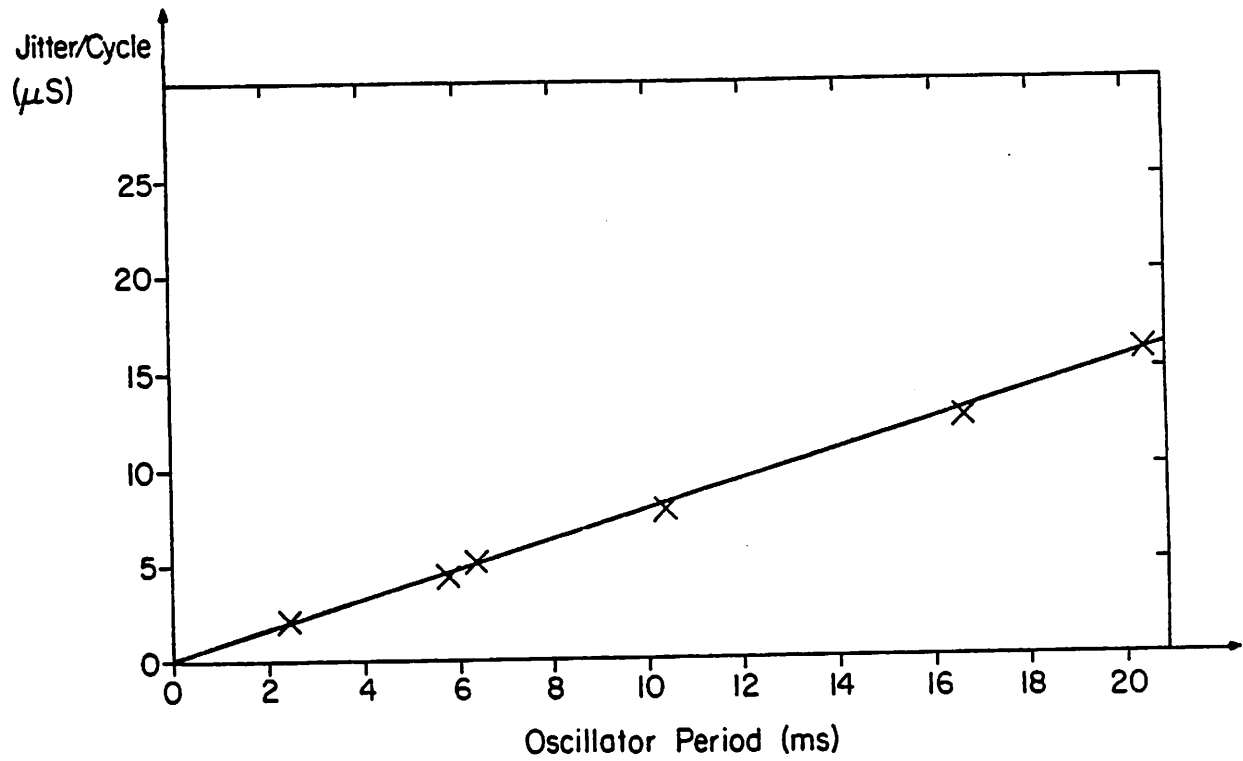


Fig. 3.9

Variation of jitter with r.m.s. noise,  
constant frequency of oscillation



**Fig. 3.10**

**Variation of jitter with frequency of oscillation,**

**constant r.m.s. noise**

interpreting its solutions; in fact, because of its complexity, this is precisely what we have tried to avoid throughout this study. However, under the assumptions that *the switching time is negligible compared to the relaxation time* and *the noise is broadband*, some very useful results can be obtained. These assumptions amount to saying that the parasitics should be much smaller than the timing capacitor, and the bandwidth that the noise is subject to prior to the regenerative element should be wide enough so that the maximum slew rate of noise the timing ramp rate.

Under these conditions, we can make a *quasi-static model* of noise in the circuit near regeneration. Consider the complete switching trajectory of  $i$  from relaxation, through the active region, into regeneration.  $di/dt$  is small near relaxation, and to the rapidly varying noise, the circuit appears linear whose gain and bandwidth are slowly varying with time. As  $i$  increases in the active region, so does  $di/dt$ , until the latter becomes equal to the maximum slew rate of the noise; because the circuit parameters vary at the same rate as the noise, steady state assumptions no longer apply. If this happens at  $i = I_f$ , the noisy current trajectories look like those in Fig. 3.11. For  $i > I_f$  the superimposed noise has no effect, while the *noise fluctuation at  $i = I_f$  is the final arbiter of the time  $T$  when  $i = I_f$* . Therefore, the bandwidth of the circuit biased at  $I_f$  should be the noise bandwidth.

Where is  $I_f$  relative to  $I_r$ ? If we straightforwardly interpret its definition that is,

$$\{ \text{Noisedensity} \times \text{Gain} \times \sqrt{\text{Bandwidth}} \} \times \{ 2\pi \text{ Bandwidth} \} \text{ (at } I_f) = \frac{di}{dt} \text{ (at } I_f)$$

then by doing a series of small signal analyses we can find the appropriate bias point at which this inequality is satisfied. However, it is disconcerting to observe that this bandwidth depends on the noise level.

Let us examine how sensitive  $I_f$  is to the noise power. We seek the small-signal transfer function of  $v_n$  onto  $i$ , that is,  $di/dv_n$ . From the chain rule,

$$\frac{di}{dv_n} = \frac{di}{dt} / \frac{dv_n}{dt} = f(i) / \frac{dv_n}{dt}$$

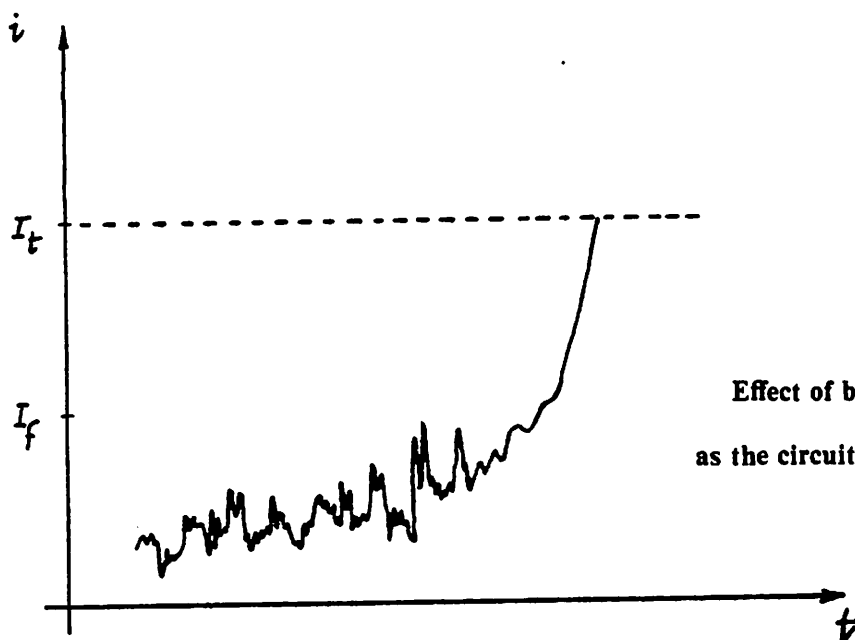


Fig. 3.11  
Effect of band-limiting of noise,  
as the circuit approaches regeneration

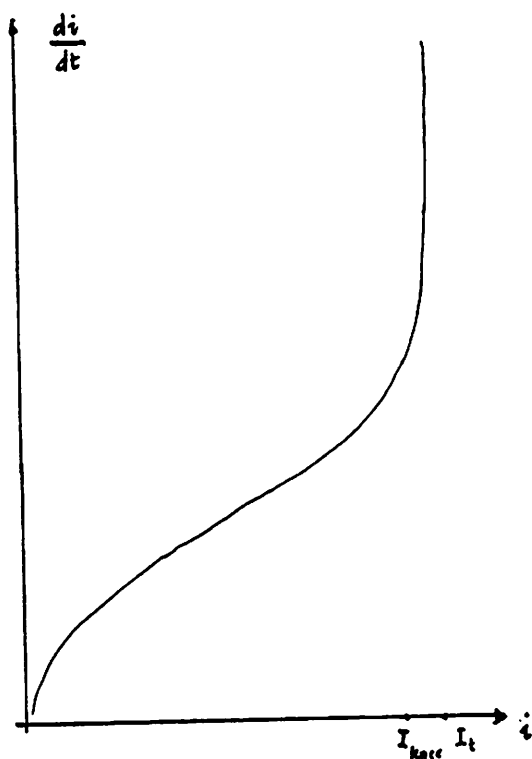


Fig. 3.12  
Variation of  $di/dt$  with  $i$  for AD 537 V.C.O.

where  $f(i)$  is the R.H.S. of (3.4). Now  $dv_n/dt$  is fixed by the input noise, so  $di/dv_n$ 's dependence on  $i$  is proportional to  $f(i)$ . A plot of  $\log_e f(i)$  vs.  $i$  is given in Fig. 3.12; observe that  $f(i)$  increases rapidly past a knee in the curve, and the knee ( $I_{knee}$ ) can be estimated by a piecewise linear approximation to the curve. Due to the rapid increase of  $di/dt$  at  $I_{knee}$ , the variation of  $I_f$  with noise power shall be small. In other words,  $I_f = I_{knee}$ .

All relaxation oscillators have a similar knee due to the regenerative element, which will, in general, introduce a term of the type  $(I_f - i)^m$  in the denominator of  $f(i)$ .

### Experimental results

The noise bandwidth of the core of the AD 537 E.C.O was measured experimentally using a modified noise injection method. We expected this bandwidth to be large, because it is a connection of six emitter followers with capacitive loading at the output, which produces zeros in the s-plane leading to peaking in the small signal frequency response. Ideally, the noise bandwidth could be estimated by a series of experiments consisting of injected noise of a fixed r.m.s. value, but with increasing bandwidths; the jitter produced by the noise would decrease once the noise bandwidth was exceeded. However, the noise generator available to us had a maximum usable bandwidth of 50 kHz; by amplitude modulating a high frequency carrier with it, we heterodyned it up to the required frequency range. When injected into the AD 537, the jitter in response to the centre frequency of this signal is shown in Fig. 3.13. The rolloff is around 10 MHz.

The small signal frequency response of the AD 537 was simulated on SPICE, with the circuit biased at  $I_f$ , the timing capacitor shorted at a.c. and using the device models of CHAPTER 4. A rolloff frequency of 6 MHz was obtained.

There are two major differences in these results. First, while the simulation predicts a rolloff rate of 20 dB/decade, the measured rolloff is much steeper. Second, the measurements show a small peak at 20 MHz, whose height increases with the amplitude of the injected signal. Although we cannot explain this, it is due to the slight dependence of the noise bandwidth

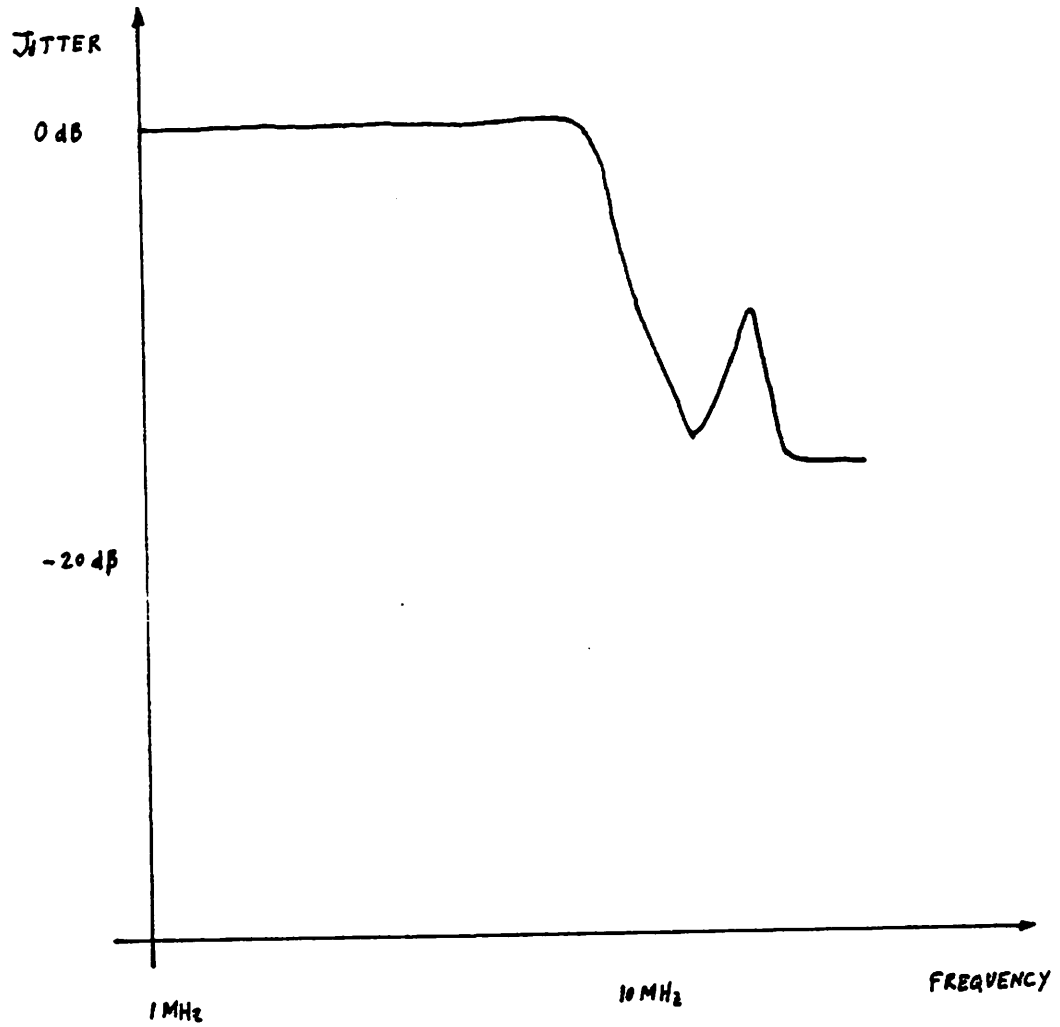


Fig. 3.13

Noise bandwidth of AD 537 V.C.O.

---

model on the signal level.

### Generalisation of results

The preceding results not only add to our understanding of relaxation oscillators, but to all regenerative circuits. For example, noise in a flip-flop (bistable) circuit driven by some input waveform can now be analysed. A flip-flop acts just like a Schmitt trigger, except that it is not driven by slowly varying waveforms as in timing circuits, but by edges of pulses, which vary rapidly; consequently, jitter is never an issue. For example, even though the input stage of a T.T.L. flip-flop has an equivalent input thermal noise voltage of about  $6\text{ k}\Omega$ , this matters little when the flip-flop is used to divide down very low jitter frequency sources. The divided frequency preserves the stability of the source, no degradation being introduced by the divider circuits, because each one is driven by a pulse. An exception is the first divider which may be driven by a sine wave output from the frequency source; the slope of this at its zero crossing is  $2\pi \times \text{amplitude} \times \text{frequency}$ , so a large amplitude will reduce any jitter due to this divider.

The results apply equally well to relaxation circuits with exponential and other timing waveforms, where the jitter is determined by the slope at the trigger threshold.

Now we can justify the oscilloscope method of measuring jitter described in CHAPTER 2. The Time Base oscillator (a relaxation oscillator) of the oscilloscope is capable of jitter, but it is triggered by fast pulses obtained from the output of the Trigger Level voltage comparator. This, in turn, when triggering on the transition of our square wave, is driven by the large slope of this transition. Consequently, even if this voltage comparator had a substantial input noise, it would produce a very small jitter in the Time Base oscillation.

## Accuracy of the switching model

How accurately does the First Crossing model correspond to the physical process of switching? To cause premature triggering, a noise peak must initiate regeneration in the circuit by conveying enough energy into some active device. For a bipolar transistor, this means that the noise peak deposits a suitable charge of minority carriers into its base. The farther away the circuit is from its "natural" regeneration point, the greater must be this charge. To understand the circuit's response to noise peaks, let us model the noise as randomly spaced unit impulses. A Schmitt trigger, biased in its active region short of its regeneration, when driven by a small impulse will produce a slowly decaying response, as shown in Fig. 3.14. This will be an outcome of the charge storage dynamics of the input device of the Schmitt. If the impulse is large enough, however, the current of the device turning ON can exceed the threshold,  $I_r$ , and put the circuit into regeneration.

The active devices and parasitic capacitors in the Schmitt determine a non-zero energy input for  $i$  to exceed  $I_r$ . Thus, the noise may exceed the threshold at the circuit input *many times* before  $i(t)$  actually switches. This does limit the usefulness of the First Crossing model if it is to be used to predict the precise instant of a transition. However, the statistics of switching still obey this model, because, if we refer our attention to the Schmitt current, it does indeed regenerate after it first crosses the threshold. That is, many noise spikes crossing at the input stimulate one crossing of the output variable. This is why the distribution of the jitter is remarkably uniform over a wide variety of circuits, all of which consist of active devices of widely varying dynamical properties (i.e. speeds).

We must also include the energy storage requirements of the active devices which precede the Schmitt, and their associated parasitic capacitances. Thus, before it causes switching, noise superimposed on the ramp must provide enough energy to all the devices which exist between itself and the Schmitt output.

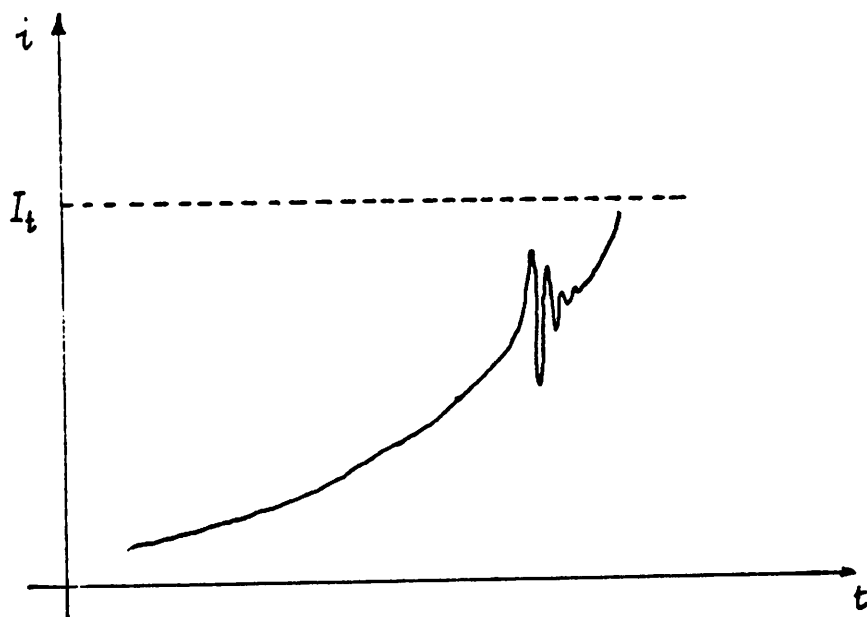


**Fig. 3.14**

**Impulse response of Schmitt trigger**

**biased near regeneration**

---

## C H A P T E R 4

---

### The Statistics of Phase Jitter

Considering the effort that has gone into attempting to solve the First Crossing Problem, to hope to obtain a closed form solution for the statistical distribution of phase jitter is futile. This is not to imply that this problem is insoluble, but rather that it is outside the scope and interest of the circuit designer, whose main intent is to reduce the variance of the pulse periods, whatever the details of their distribution may be.

Middleton [19] appears to be the first to have posed and attempted to solve the problem of spurious triggering of ideal comparators due to the noisy input waveforms. The inputs were square waves, and would trigger the comparator during their transition, which was modelled as a ramp. For the input a certain distance away from the comparator threshold, Middleton calculated the *expected number of crossings* by the noise, indicating the susceptibility of the circuit to spurious triggering.

Estimating the probability of the *first crossing* is a different matter though, and this is what we require for the triggering of our regenerative circuit. Such an estimate must consider the dynamics of the ramp as well as the bandwidth of the noise. More precisely, if the driving ramp is  $I_d$  below the threshold,  $I_t$ , at time  $t$  (Fig. 4.1), then we require the probability of (No crossings of  $I_t$  by the noise on the ramp in the interval  $(0, t)$  and a crossing in the increment  $(t, t+\delta t)$ ) for various values of  $I_d$ <sup>11</sup>. Methods similar to Middleton's could be used, but we did not find any convenient means of doing the integrations.

Both the noise power and its bandwidth will be important, for in a given bandwidth, a large noise power will be more likely to cross the threshold, but conversely, for a given power a

---

<sup>11</sup>For noise of finite bandwidth, as  $\delta t \rightarrow 0$ , there can at most be one crossing.

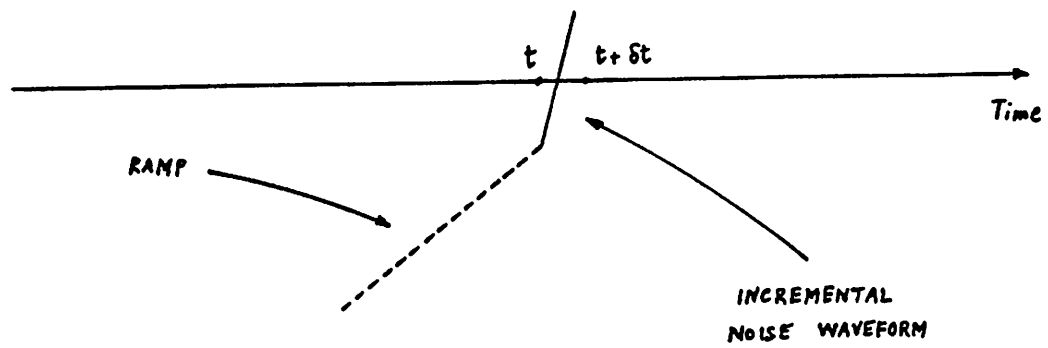


Fig. 4.1

The requirements on the magnitude and slope of the noise waveform to make first-crossing in time increment

broader bandwidth will produce a greater rate of change and increase the likelihood of crossing the threshold. The experimental investigation of these ideas is described in the remainder of this chapter.

To clarify the process, we consider the ramp to be noiseless, and the threshold to have noise superimposed on it. The slope of the noise satisfies a distribution whose variance is determined by the noise bandwidth, thereby making it extremely improbable for the slope to be greater than a certain magnitude. For example, if  $dv_n/dt$  satisfies a Gaussian distribution, we can assume that  $|dv_n/dt| < 3\sigma$  with a 99.97% probability [17]. Let us call this "limiting" slope  $\dot{v}_{nmax}$ . For white noise with density  $\hat{v}_n$  and a single pole rolloff at bandwidth  $B$

$$\dot{v}_{nmax} = \hat{v}_n \sqrt{B} \times 2\pi B \quad (4.1)$$

We can think of this quantity as the *maximum slew rate* of the noise, while emphasising again that this is practically a maximum value even though with a vanishingly small probability the slope can be arbitrarily large.

First consider the case when the ramp slope is much greater than the maximum slew rate of the noise. Over a large enough series of intersections, the ramp will uniformly explore the complete noise waveform (Fig. 4.2(a)); that is, the first-crossing instants will be proportional to random samples of the noise, the proportionality being true because the ramp is linear. Thus, the distribution of the resulting jitter will be the same as that of the noise, and

$$\sigma(T) = \frac{\sigma(v_n)}{\lambda} \quad (4.2)$$

where  $\lambda$  is the slope of the ramp.

On the other hand, the maximum slew rate of the noise may be greater than the ramp rate, either due to a wide noise bandwidth or large noise power. In this case, the first crossing will *almost always occur at a positive noise peak* and almost never near its mean value (Fig. 4.2(b)).

This results in only one of the tails of the noise distribution being sampled, so that

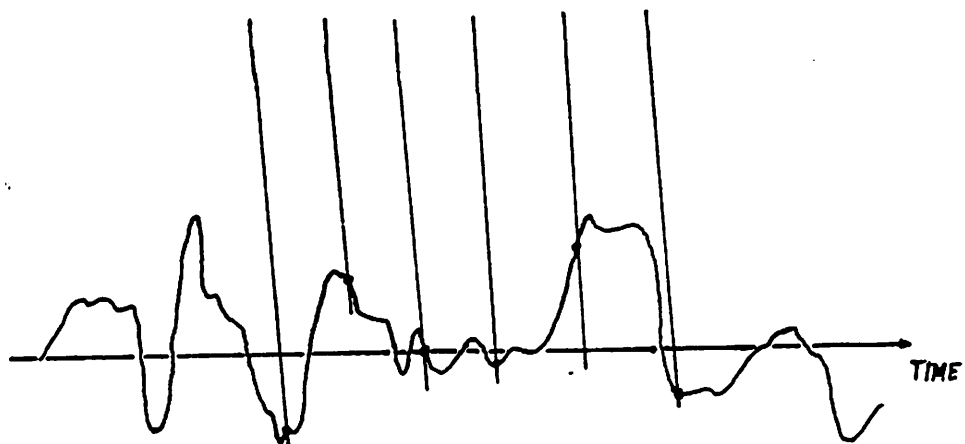


Fig. 4.2(a)

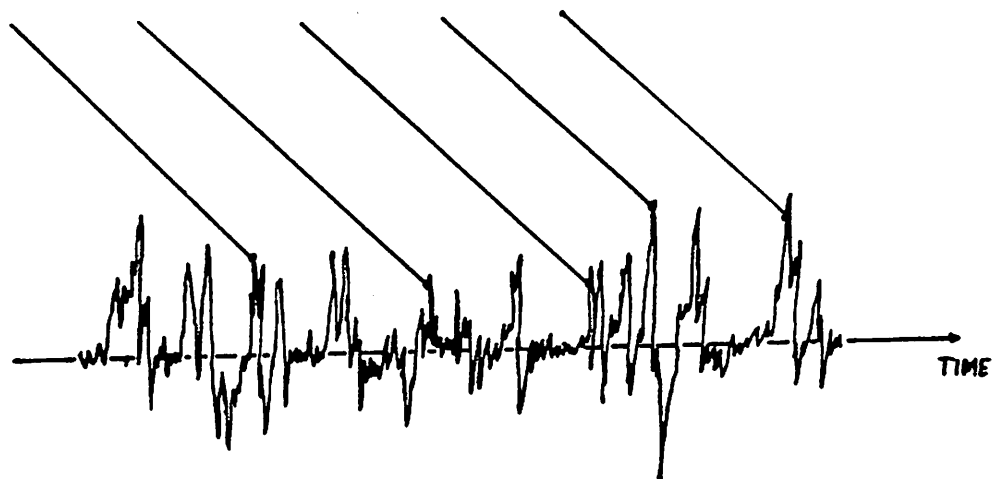


Fig. 4.2(b)

**Spread of first-crossing instants for low bandwidth  
and high bandwidth noise waveforms**

$$\sigma(T) < \frac{\sigma(v_n)}{\lambda} \quad (4.3)$$

From the illustration of the first crossing process in Fig. 3.5, it is evident that even though the inequality in (4.3) is true,  $\sigma(T)$  is *proportional* to the R.H.S.; call this constant of proportionality  $\alpha$ . In (4.2), when  $\dot{I}_{nmax} \ll \lambda$ ,  $\alpha = 1$ ; it is plausible to expect that it tends to some asymptotic value less than 1 when  $\dot{I}_{nmax} \gg \lambda$ . Extensive data obtained from two different oscillator circuits revealed this asymptotic value to be about 0.5. If we define  $\omega_N = \frac{\dot{v}_{nmax}}{\lambda}$ , the variation of  $\alpha$  with  $\omega_N$  of Fig. 4.3 results, with a fairly sharp transition between the two asymptotes at  $\omega_N=1$ .

Histograms of the jitter were obtained from accurate measurements of single cycles of oscillation for various values of  $\omega_N$ . For  $\omega_N \ll 1$ , the histograms are symmetrical and fit a Gaussian function well, as expected (Fig. 4.4). For  $\omega_N \gg 1$ , the histograms, when plotted on a normalised scale, did not change measurably (Fig. 4.5). It appears that for a small noise, the distribution remains Gaussian.

The *mean* frequency due to the presence of noise when  $\omega_N \gg 1$ . This is due to the premature first crossing of the ramp with the threshold that almost always results in the presence of noise, and if  $T$  is the period of oscillation, then

$$\delta T = -\frac{v_n}{\lambda} \quad (4.4)$$

### Measurement methods for jitter statistics

Obtaining reliable statistics from most oscillator circuits is not an easy task, primarily because this requires a large number of independent measurements of the period, and the oscillation frequency can drift over the course of the measurement by an amount greater than the data sought. In our experiments, the frequency of oscillation was stabilised by referencing it to a crystal derived frequency in a P.L.L. However, the slightest instability in the loop or

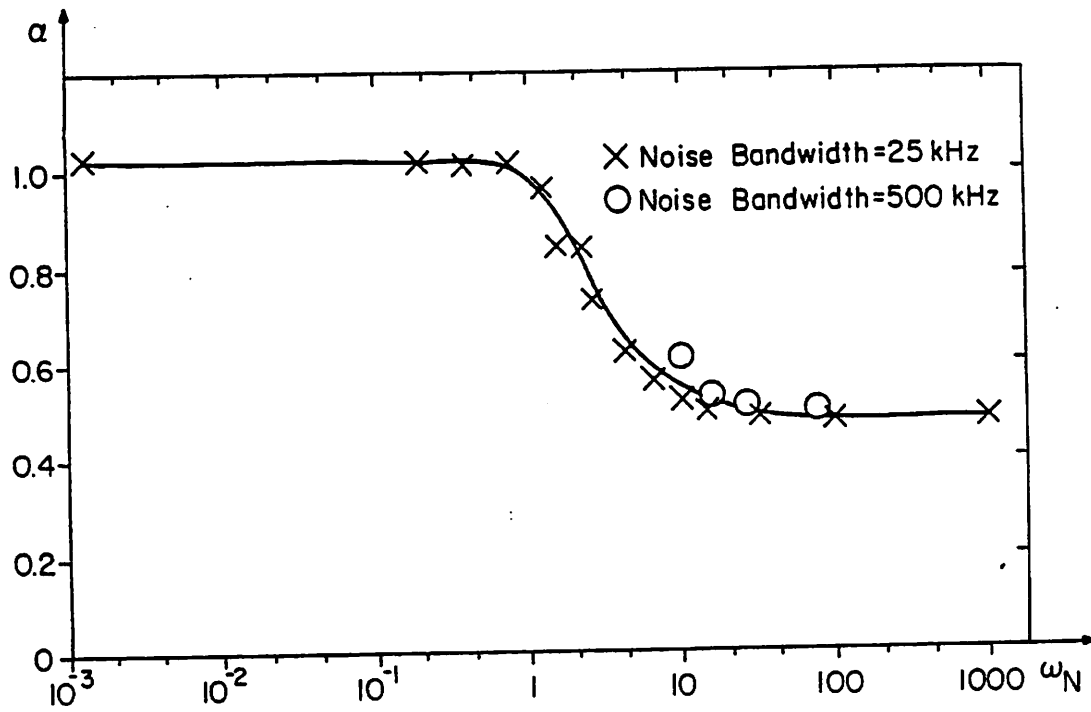


Fig. 4.3

Variation of  $\omega_n$  with  $\alpha$

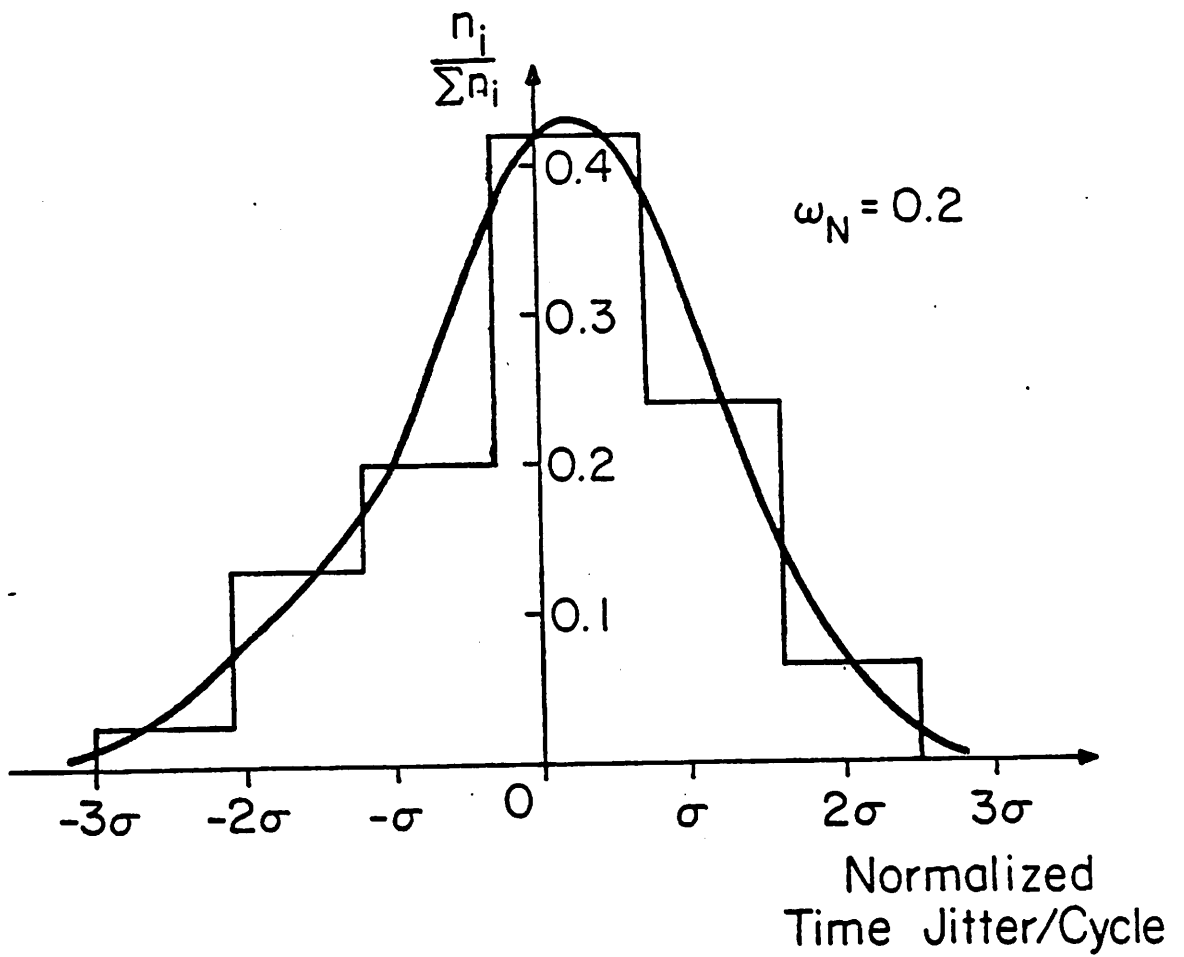


Fig. 4.4

Histogram of pulse periods, small  $\omega_n$ 

Normalised scales

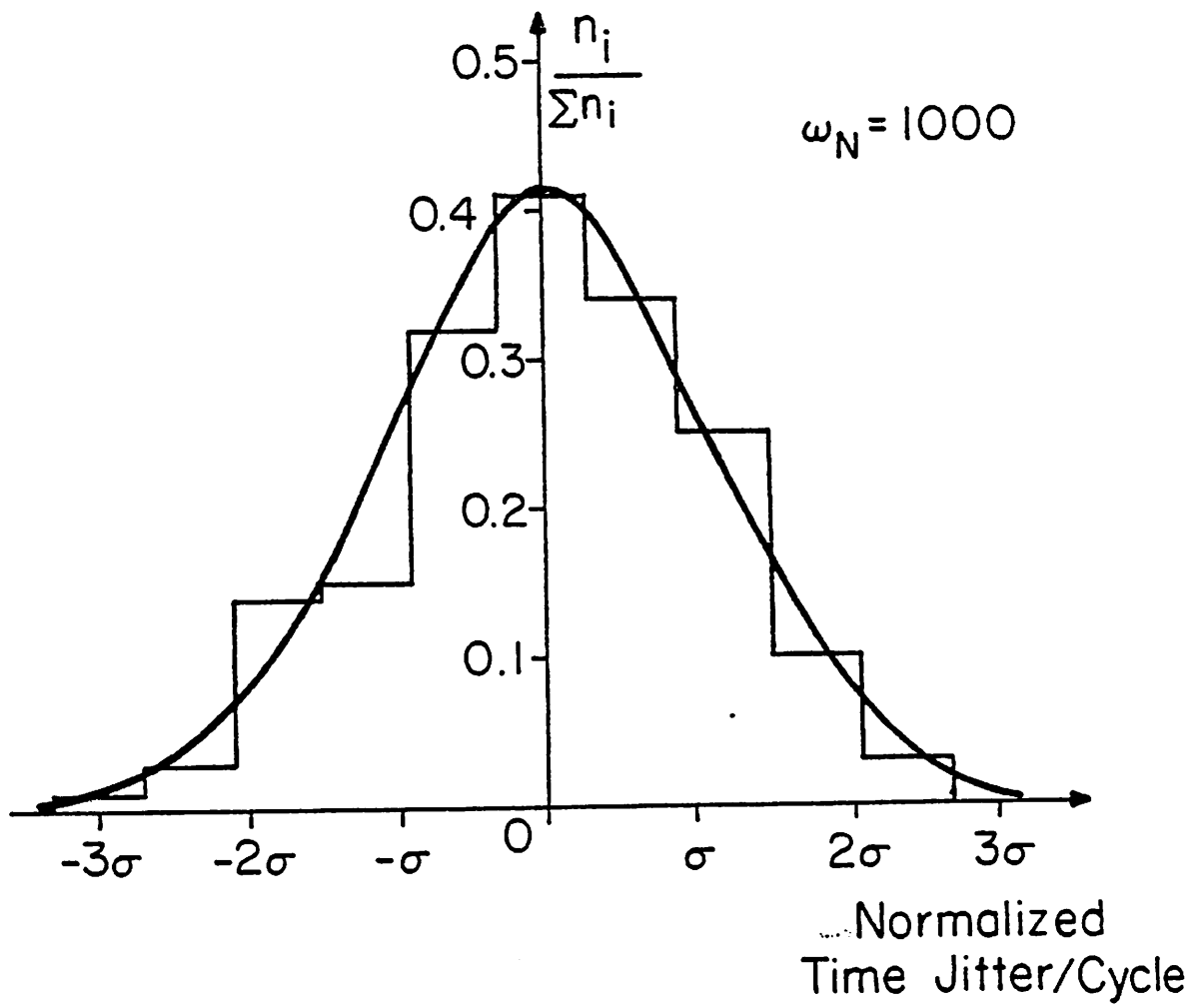


Fig. 4.5

Histogram of pulse periods, large  $\omega_n$

Normalised scales

asynchronous feedthrough to the V.C.O. control input could produce grave errors.

The measurement system is shown in Fig. 4.6. Most laboratory frequency counters can only resolve down to 10ns, so the V.C.O. was made to run at a large period ( $T$ ) like 10ms, thereby extending the  $\Delta T$  jitter well into the measurement range of the counter. The data consisted of single cycle periods obtained by manual triggering of the counter, thus ensuring that the noise in each measurement was uncorrelated; an automated measurement scheme which obtained statistics from the variance of consecutive cycles might ignore slow changes due to flicker ( $1/f$ ) noise.

Another source of inaccuracy in this measurement scheme was the feedback signal in the loop, which tried to correct the V.C.O. frequency from cycle to cycle. As an example, the histogram of Fig. 4.7 shows a decided asymmetry in favour of smaller periods, and while it had the same variance as one obtained without the loop, the latter was symmetrical about its mean value. The feedback signal could be reduced by greater filtering, at the expense of a smaller margin of stability in the loop. The most satisfactory data was obtained when an intrinsically low drift oscillator like the AD 537 was used without a loop.

If the injected noise was to serve as a large signal model of the intrinsic noise in the circuit, it was essential to use a true Gaussian noise generator<sup>12</sup>, rather than one which derives pseudo-random noise from binary sequences. The two differ most in the tails of their distributions, because the latter has severely truncated tails compared to white noise, and the jitter production is most sensitive to the peaks of the noise waveform.

To accurately predict jitter, the appropriate  $\alpha$  had to be used as follows:

$$\sigma(T) = \alpha \frac{v_n}{\lambda} \quad (4.5)$$

We found that circuits could have either of the asymptotic values of  $\alpha$  for typical magnitudes of noise power and bandwidth; both these variables had to be known in advance to calculate  $\omega_N$ .

<sup>12</sup>Like the General Radio GR 1390B.

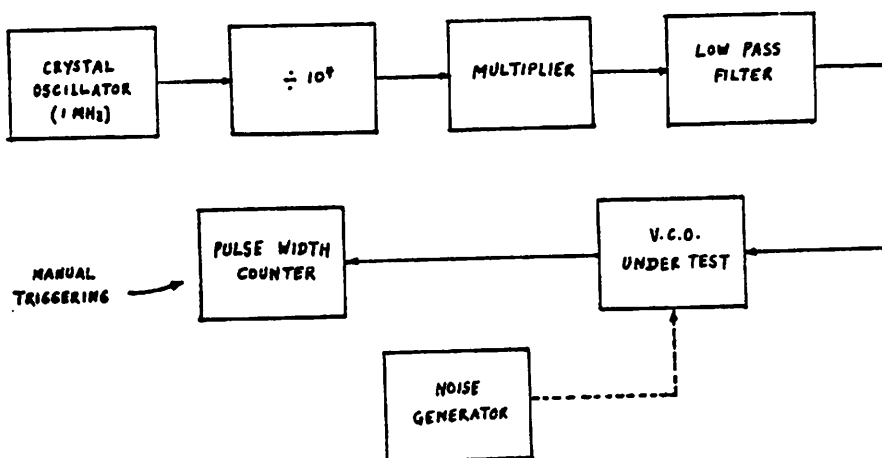


Fig. 4.6

Measurement setup for obtaining data on jitter statistics

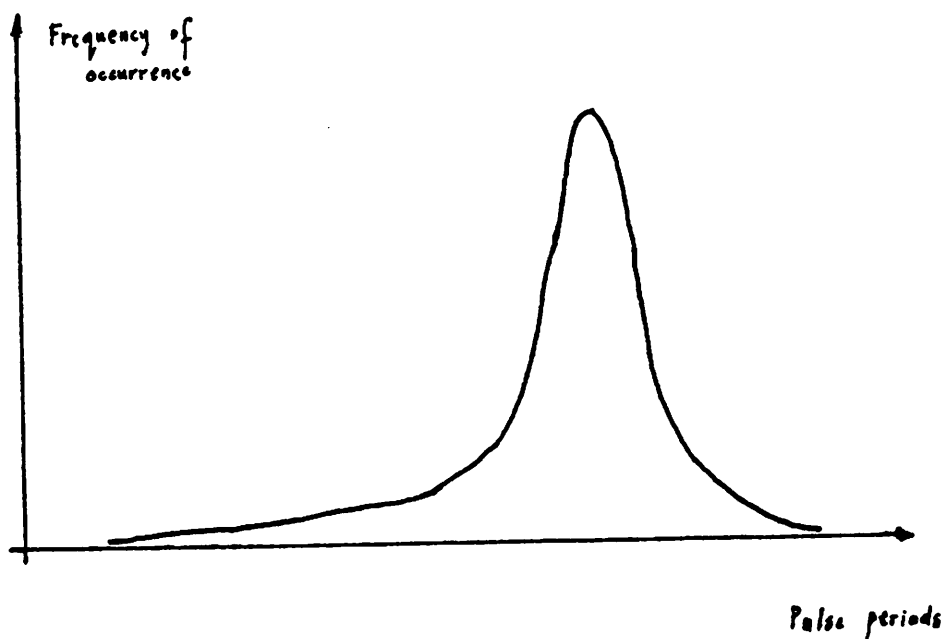


Fig. 4.7

Asymmetrical histogram due to P.L.L. feedback

### Examples of predicting jitter

1. *The AD 537 V.C.O.* This circuit, shown in Fig. 4.8, was simulated on SPICE with the following assumptions:

<i>NPN transistors</i>	<i>PNP transistors</i>
$\beta$ 100	30
$r_b$ 200	300
$\tau_f$ $12 \times 10^{-10}$	$3 \times 10^{-8}$

Using the methods of CHAPTER 3 of biasing the circuit near regeneration, the noise bandwidth was calculated to be 6 MHz and at the same bias point the equivalent noise density,  $\hat{v}_n$ , was  $1.3 \times 10^{-8}$  V/ $\sqrt{\text{Hz}}$ . The noise analysis was done with a very large value for the timing capacitor to prevent it from introducing a low frequency rolloff into the circuit, because its action is already contained in the analysis leading to the jitter formula (3.6). The output variable for the analysis was the emitter current of the transistor about to turn ON. With the peak-to-peak triangle wave of 1.8 V, and at  $f_{osc} = 1$  kHz, we get  $\omega_N = 83$ , so that  $\alpha = 0.5$ . Then, from (4.5), the r.m.s. jitter per cycle = 45 p.p.m. The measured value was 35 p.p.m.

2. *The NE 562 E.C.O.* A simplified circuit diagram of this oscillator is given in Fig. 4.9. The major sources of noise here are the Zener diodes used for level shifting, where the noise measured in a 10 MHz bandwidth was about 200  $\mu\text{V}$  per diode. The two Zener diodes contribute to the jitter in different ways. Z1 at the common collectors presents a common mode voltage to the (topologically symmetrical) circuit but as the currents are quite different in the two halves of the circuit near regeneration, it does add some noise to the ramp. If the output resistance of the timing current sources is  $r_o$ , then the noise in series with the capacitor is

$$v_n = \frac{g_m(Q14)}{g_m(Q11)} \cdot \frac{R}{r_o} v_{Z1}$$

where Q11 is assumed to be turning ON, and the circuit is biased at its regeneration threshold.

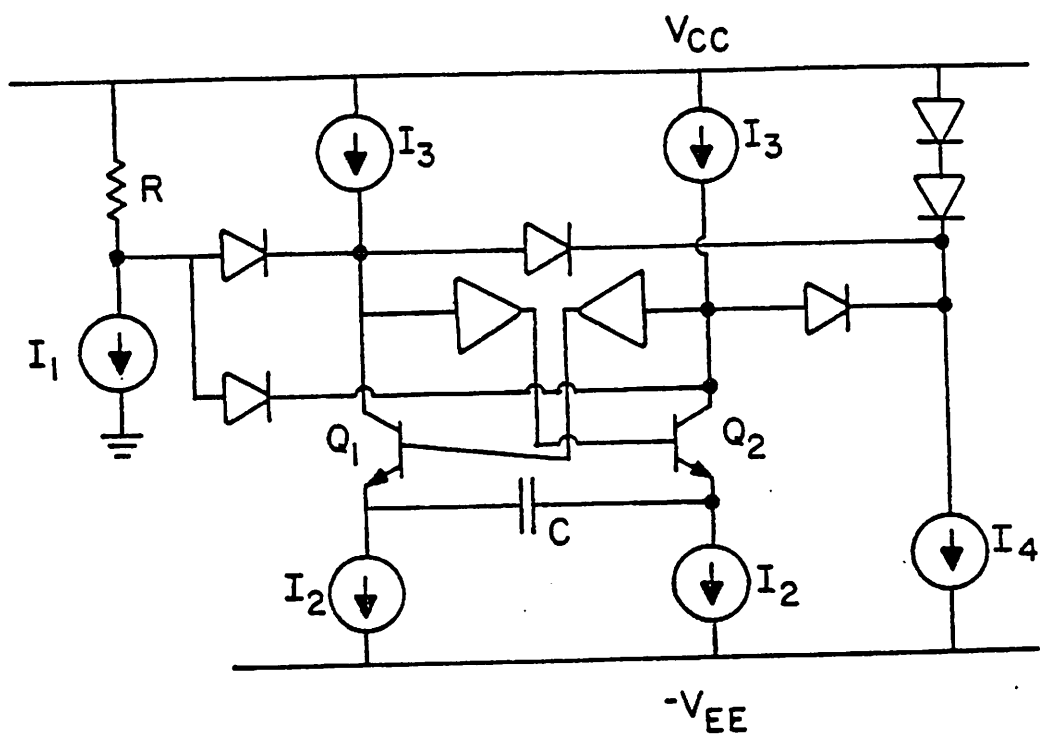


Fig. 4.8

Simplified circuit of the AD 537



Z2, whose purpose is to level shift down to the control current source, produces a noise current in Q22, which gets converted to a noise voltage

$$v_n = \frac{R_2}{R_1 + R_2} \cdot \frac{V_T}{I_0} g_m(Q22) v_{z2}$$

This is the most significant noise contribution, and we can estimate the jitter it produces by assuming  $R_1 = R_2$ ,  $I_C(Q22) = I_0$ , the noise bandwidth = 10 MHz and  $\alpha = 1$ , whence

$$Jitter = \frac{200 \times \sqrt{6} \times 10^{-6}}{2 \times 1.2} = 200 \text{ p.p.m.}$$

where the 1.2 V in the denominator is the triangle wave amplitude. Although this is a rough estimate, it agrees well with the measured value (Table 1).

The deficiencies of this circuit are clear: the Zener diodes introduce a large noise, and the triangle amplitude is small, both factors contributing to an increased jitter.

*3. The NE 565 G.C.O.* We only consider the Schmitt trigger of this circuit in Fig. 4.10.

The main sources of thermal noise in the circuit are the resistors  $R_1 - R_4$ , which are probably a few kilohms, their values not being specified in the data book; the transistors in the followers and the Schmitt trigger; and the diodes. The purpose of these diodes is to prevent the Schmitt trigger from saturating, but they only worsen the jitter by transmitting the noise in the elements of the rest of the circuit into the Schmitt. With a triangle amplitude of only 2 V, the relatively large noise produces a large jitter.

In our appraisal of oscillators thus far, we have ignored the effect of noise in the timing current sources. Let us compare the jitter produced by the thermal noise due to  $r_b = 100 \Omega$  appearing in series with the timing capacitor, with the same source of noise in the transistors comprising the timing current mirror. The following assumptions are made:  $V_\Delta = 2 \text{ V}$ ,  $I_0 = 1 \text{ mA}$ , Noise bandwidth = 10 MHz and  $T = 1 \text{ ms}$ . The r.m.s. noise due to the resistance will be  $4 \mu\text{V}$ , which will produce a jitter of 5 p.p.m.

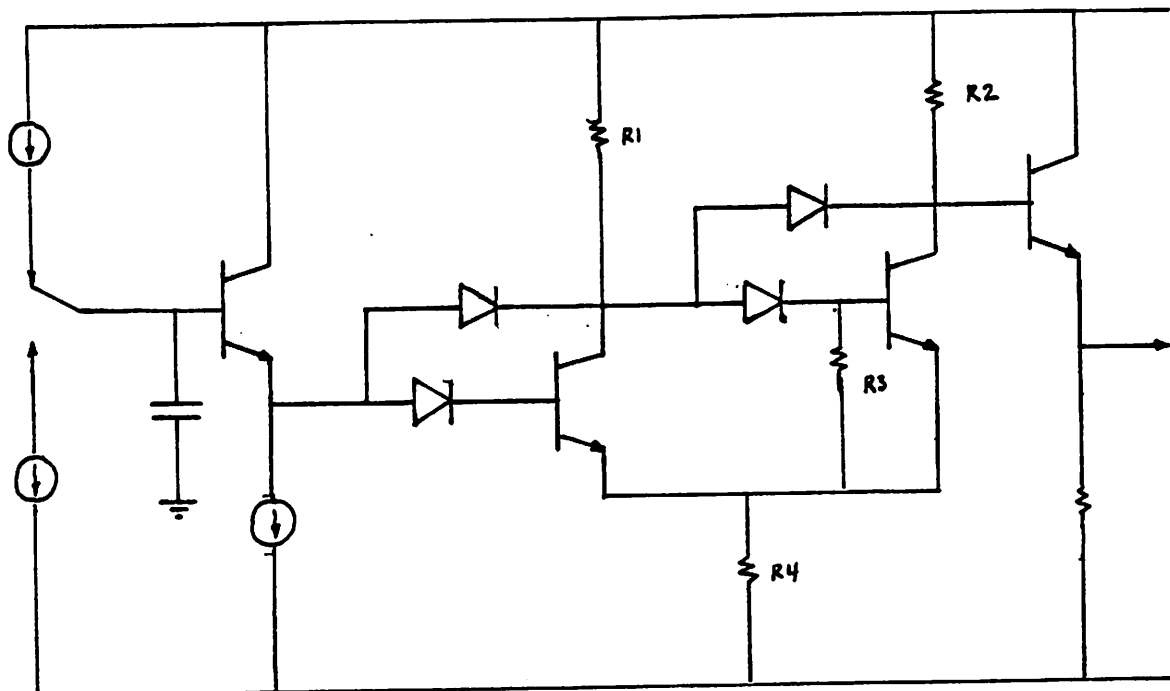


Fig. 4.10

Simplified circuit of NE 565 G.C.O.

---

Noise at the bases of a current mirror is amplified as shown in Fig. 4.11, so that the output noise is

$$i_n = g_m v_n = \frac{I_0}{V_T} v_n$$

For the values above, the output noise density is  $\hat{i}_n = 5.2 \times 10^{-11} \text{ A}/\sqrt{\text{Hz}}$ , so from (3.12)

$$\text{Jitter} = \sqrt{6} \frac{i_n}{I_0} \sqrt{T} = 4 \times 10^{-3} \text{ p.p.m.}$$

Normally, as this calculation shows, the current noise makes a negligibly small contribution to the jitter. For very large  $T$  or small  $I_0$ , however, it may become important.

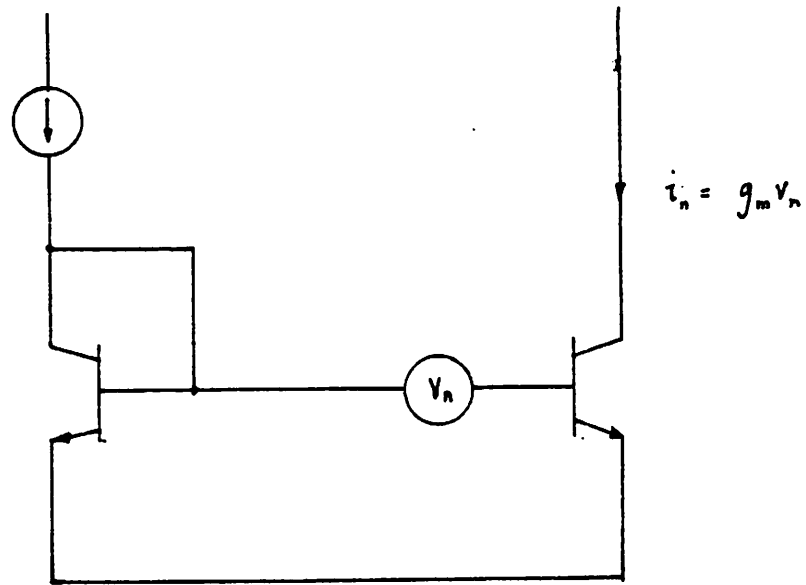


Fig. 4.11

Current mirror noise

---

## C H A P T E R 5

---

### Low Jitter Oscillator Circuits

From the theory of jitter, and the examples considered above, the criteria for low jitter design have become evident, and can now be simply stated. The significant contributions to jitter are made by the noise sources which appear in series with the slowly varying signals, while the noise driven by fast slopes makes a small (and often negligible) contribution. This separation of the circuit into sections defined by the time scale of the signals present there is called *hierarchical decomposition*, and is an important first step in the analysis of such circuits. For example, we always assume that in the G.C.O. the voltage on the timing capacitor and the emitter follower is constant while the Schmitt trigger switches between its two states. Thus, the slow part of the circuit is in a steady-state while the the fast one is in motion.

At a given frequency of oscillation, the jitter is reduced by increasing the slope of the timing ramp. This can be done either by increasing the amplitude of the triangle wave, or by suitable waveform shaping. Let us consider the second alternative first.

Suppose in a G.C.O. that the Schmitt is directly driven by the timing capacitor ramp. The slope of the ramp only matters when the Schmitt is in its active region, if the slope were to be increased during this short interval of time, it would reduce the jitter proportionally without greatly altering the period of oscillation. This could be realised using a wave-shaping circuit (Fig.5.1) with a suitably non-linear transfer characteristic. Were this scheme to be implemented, however, we would observe little or no change in jitter; for, having rendered the noise in the Schmitt ineffective, the noise at the wave-shaper's input would instead appear in series with the ramp. In short, the approach is futile, because we simply transfer the problem from one part of the circuit to another, without ever getting rid of it.

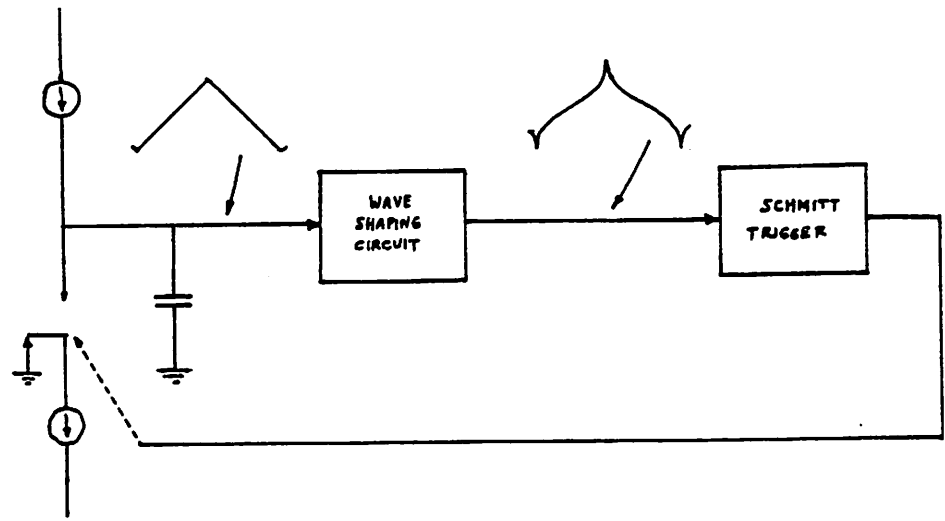


Fig. 5.1

Circuit for driving the Schmitt trigger with large slopes

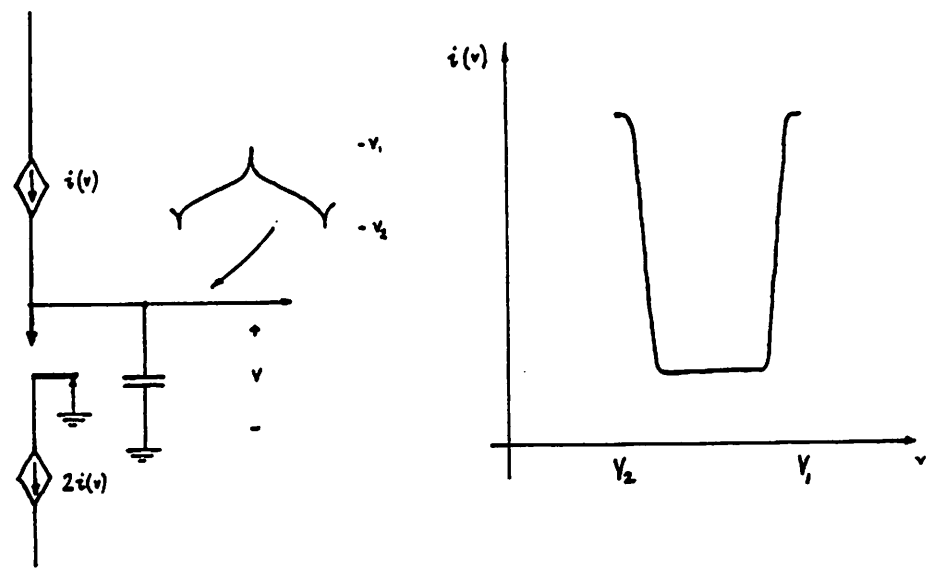


Fig. 5.2

Producing a cusped voltage on the timing capacitor,  
and the voltage dependent current source characteristics

In principle, however, a significant improvement could be brought about if the ramp on the capacitor were replaced by another timing waveform which, intrinsically, had sharp edges in the Schmitt's active region. The capacitor voltage would then be a cusped triangle as in Fig. 5.2, but the "current source" required to produce it would be a non-linear resistance with a "well" characteristic. There being no straightforward way of synthesising this, the scheme remains a hypothetical one.

The first alternative is more practical, where a linear ramp with a large amplitude is used, and, additionally, the noise in series with it is minimised. This led to the circuit described below.

To minimise the noise on the ramp, we consider the oscillator topology which will permit the least number of active devices in the slow time scale sub-circuit. By combining both the timing and regeneration functions, the E.C.O. necessarily involves at least six transistors, and very likely more for temperature compensation. The G.C.O., on the other hand, can be modified so that at most three transistors contribute to the noise. If a two-level comparator is inserted between the timing capacitor and the Schmitt, it can both define the amplitude of the triangle as well as the noise at the input (Fig. 5.3). The amplitude of the ramp is then the difference in the two reference voltages, and the noise is determined by the comparator input stages only. The main disadvantage of this scheme is the large propagation delay through the loop, which reduces the maximum frequency of oscillation; however, a recently published i.c. [22] shows that with careful design, an oscillator of the same species can work upto 100 MHz, certainly performing as well as any E.C.O.

Using single-stage differential pairs as comparators, the circuit of Fig. 5.4 was bread-boarded. Low noise bipolar transistors<sup>13</sup> with a specified broadband input noise density of  $2 \text{ nV}/\sqrt{\text{Hz}}$  and 600 nV of flicker noise in a 10 Hz bandwidth were used. A triangle wave of 8 V peak-to-peak was obtained using  $\pm 6 \text{ V}$  power supplies. The r.m.s. cycle-to-cycle jitter was

<sup>13</sup> National Semiconductor LM 394 supermatched pairs.

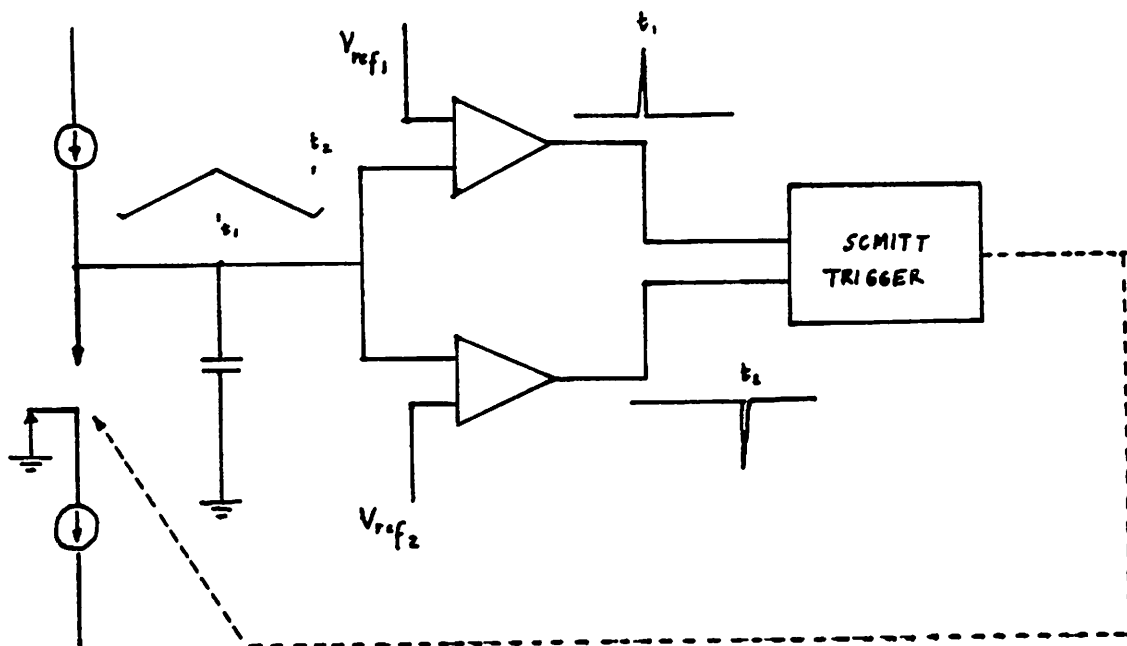


Fig. 5.3

Modified version of the basic Grounded Capacitor Oscillator



---

measured to be about 2 p.p.m. at  $f_{osc} = 1$  kHz. Discrete series diodes had to be added at the emitters to drop up to 8 V of reverse voltage, but these became the dominant noise sources in the circuit, producing about 5  $\mu$ V of flicker noise in a 100 Hz bandwidth.

The circuit was primarily meant to test the theory of jitter, and was by no means regarded as competition for general purpose V.C.O.s. Its drawbacks are a very large drift with temperature, sensitivity to power supply fluctuations (which are transmitted directly through the reference voltage resistors) and a frequency of oscillation limited below 50 kHz. Despite differential comparators, the voltage regulators noise from the power rails dominated the jitter, and it became necessary to run the final version off batteries.

To minimise power dissipation, large resistors were liberally used in the fast time scale portions of the circuit, as their contribution to the jitter was small. In fact, reducing these resistors by  $\times 10$ , and thus their noise by  $\times 3$ <sup>14</sup>, did not measurably affect the jitter. Neither did the noise in the current mirrors.

An improved version of this circuit is being tested in the continuation of this project<sup>15</sup>, which promises an improved stability, a larger maximum oscillation frequency with jitter of about 10 p.p.m. using a 5 V power supply. The improvement in stability has been brought about by using a precision voltage reference to determine the amplitude of the triangle wave, op amps with a low temperature coefficient of offset to determine the timing currents and differential comparators with a large power supply rejection.

The noise bandwidth of this breadboard circuit was, no doubt, determined by the Schmitt trigger. The comparators, though, had a bandwidth of only 50 kHz, dominated by the Miller multiplied breadboard capacitance. To simplify calculations, we assumed that the noise bandwidth was also 50 kHz. The gain of each two-stage comparator was about 50.

The jitter due to broadband noise was estimated as follows: Including the emitter follower, the total input noise is at most due to four devices, obtained by the square root of the sum of

<sup>14</sup>Assuming the noise bandwidth did not change.

<sup>15</sup>By Mr. T.-P. Liu of U.C. Berkeley.

their mean square contributions. Thus,

$$v_n = \sqrt{4} \times 2 \times 10^{-9} \times \sqrt{2 \times 10^5} = 1 \mu V$$

so at  $f_{osc} = 1$  kHz,  $\omega_N = 2 \times 10^{-4}$ , predicting

$$\text{Jitter per cycle} = \sqrt{6} \frac{10^{-6}}{16} = 0.15 \text{ p.p.m.}$$

The flicker noise in the diodes will produce a jitter of 1 p.p.m., thereby dominating the total jitter in the circuit.

When it drives a large output capacitance, the rate of the Schmitt trigger transition can be slower than expected. Therefore, if the stage following the Schmitt were very noisy, it could measurably add to the jitter. Now, the oscillation is defined by the time that the Schmitt changes state, — once this has happened, and irreversibly so, how can the following stage influence the jitter? It is through the memory on the timing capacitor that noise in the current switch affects the switching instant *one half cycle later*. That is, noise in the signal path from the capacitor to the Schmitt affects the imminent switching; noise between the Schmitt and the capacitor affects the next switching<sup>16</sup> (except that this latter effect is normally small, because it is driven by a large slope).

Finally, to reduce the jitter still further, provided it was due to wideband noise, the comparator and Schmitt bandwidths could be artificially reduced by externally loading them with capacitance. This scheme would only be useful in applications where the V.C.O. frequency was expected not to exceed some medium value, or be subject to rapid changes.

The design criteria used on the breadboard can be directly extended to integrated circuits. A few critical devices determine the equivalent noise responsible for the jitter, and this can be minimised by making their areas large. The circuit surrounding the timing capacitor should be able to withstand a voltage swing near the power supplies without saturating. Using a 5 V

<sup>16</sup>This separation is not as clear in the E.C.O.

---

power supply, it is impractical to expect a jitter less than 0.5 p.p.m., which would result from the thermal noise of about 200  $\Omega$ .

---

## C H A P T E R 6

---

### Synchronisation in Relaxation Oscillators

"... Wherefore, it seems to me you had best not be too fastidious in your curiosity touching this leviathan."

*H. Melville, MOBY DICK.*

Suppose that instead of noise, a periodic signal  $f_{in}$  was present in the oscillator circuit. It would modulate the switching instants in much the same way as noise, except that the modulation would now be *systematic*, and would depend on the frequency difference  $\Delta f = |f_{in} - f_{osc}|$ . A large  $\Delta f$  should produce a straightforward frequency modulation of the oscillator; however, it is observed that if  $\Delta f$  is less than a threshold value, the modulation disappears altogether. This phenomenon is known as *synchronisation*, so called because the two frequencies now become equal, and the oscillator's phase is in synchronism with the phase of  $f_{in}$ .

Appearing in such diverse phenomena as closely placed clocks and the flashing of fireflies, synchronisation has interested natural scientists for a long time. For example, certain species of firefly in Pacific Asia emit light as swarms in mutual synchrony, often doing so without stopping for a major portion of their lifetimes. This group behaviour, which is thought to produce an advantage in reproduction of the species, has been modelled by a simple biological relaxation oscillator (called a pacemaker) in each fly, which is responsible for triggering the light emission. Each new member of a swarm synchronises by observing the flashing of the others[23].

It appears that synchronisation is a generic characteristic of relaxation oscillators. Using the switching model of our oscillator, we now consider its response to a periodic perturbation.

Suppose  $f_{in} \ll f_{osc}$ , so that a slow frequency modulation of  $f_{osc}$  results; the depth of this modulation is

$$\delta f_{osc} = \frac{A_{in}}{\lambda} \quad (6.1)$$

where  $A_{in}$  is the amplitude of  $f_{in}$ . If, keeping  $A_{in}$  constant,  $f_{in}$  is now increased and brought closer to  $f_{osc}$ , then at some point  $\Delta f$  shall become equal to  $\delta f_{osc}$ , so that the frequency modulation can instantaneously make  $f_{osc}$  equal to  $f_{in}$ . With an appropriate phase difference between the two oscillations, this frequency shifting effect can repeat in precisely the same way in each cycle. The oscillator's transitions are then governed by the input frequency; that is, the two are synchronised.

The study of the dynamics of synchronisation is very involved, and we restrict ourselves to examining some basic issues. In particular, we consider the range of frequencies which can synchronise the oscillator (called the capture range), the number of cycles required for synchronisation to occur, and the response of the oscillator to frequencies outside the capture range. The switching model we use is summarised in Fig.6.1, where the switching instant is determined by the first crossing of a linear ramp with a periodically varying threshold. Unlike the case of white noise, the curve of the modulation index  $\alpha$  vs.  $\omega$  now decays down to zero for  $\omega \gg 1$ , because the ramp almost always crosses a periodic waveform of high frequency at the same point, its peak value, thus producing no cycle to cycle variation in  $f_{osc}$ .

To examine the modulation of the oscillator by a fixed external frequency, we mark the switching instants of the former with respect to the phase of the latter. More precisely, we define the Poincaré map  $F$  [24], which maps the phase of  $f_{in}$  at the start of a relaxation cycle ( $\theta_0$ ) to that at the end ( $\theta_1$ ), that is,  $F : \theta_0 \rightarrow \theta_1$ . Using the switching model of Fig.6.1, we can write  $F$  explicitly for a sinusoidal input as follows:

$$T_1 = \frac{V_{\Delta}}{\lambda} + \frac{A_{in}}{\lambda} \sin \theta_0 - \frac{A_{in}}{\lambda} \sin(\theta_0 + \omega_{in} T_1) \quad (6.1)$$

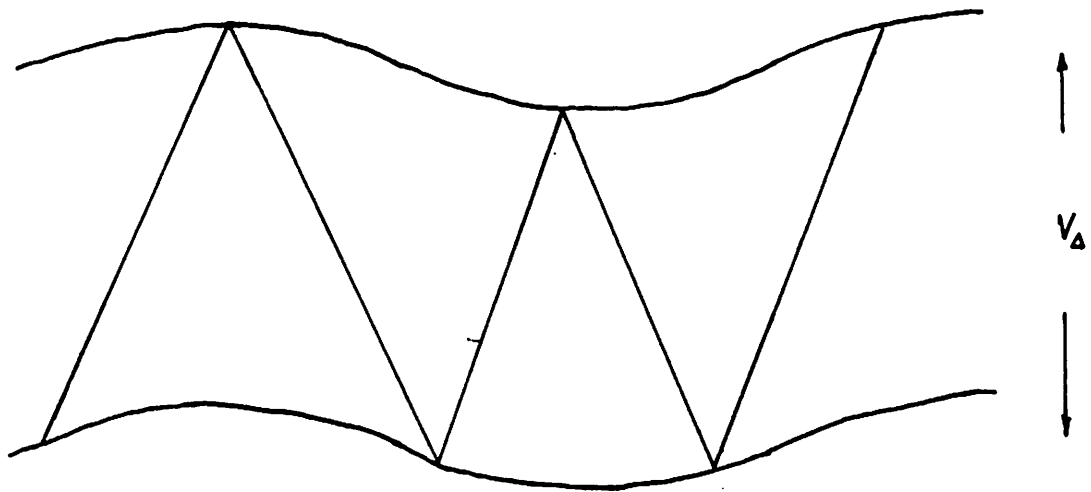


**Fig. 6.1**

**Model of switching in the presence of a periodic excitation**

$$T - T_1 = \frac{V_\Delta}{\lambda} - \frac{A_{in}}{\lambda} \sin(\theta_0 + \omega_{in} T_1) + \frac{A_{in}}{\lambda} \sin(\theta_0 + \omega_{in} T) \quad (6.2)$$

$T$  can be obtained from these equations by eliminating  $T_1$ , whence

$$F(\theta_0) = \theta_T = \theta_0 + \omega_{in} T \pmod{2\pi} \quad (6.3)$$

To investigate periodic solutions, we study the iterates of the map  $F$  on the interval  $[0, 2\pi)$ , that is,  $F(\theta)$ ,  $F(F(\theta))$ ,  $\dots$ , where the  $k^{\text{th}}$  is written as  $F^k(\theta)$ . If there exists a *fixed point* of  $F$ , or of some  $F^k$ , then a periodic solution of period  $k$  exists, as defined below.

We now investigate the properties of  $F$  as prescribed by (6.1) to (6.3), assuming  $A_{in}$  is small compared to  $V_\Delta$ ; this is almost always the case in practice. If, in addition,  $f_{in} \sim f_{osc}$ , then (6.1) may be written

$$T_1 = \frac{V_\Delta}{\lambda} + \frac{A_{in}}{\lambda} \left\{ \sin(\theta_0) - \sin\left(\theta_0 + \omega_{in} \frac{V_\Delta}{\lambda}\right) \right\}$$

with an error in the last term of  $o(\omega_{in} A_{in}/\lambda) = o(A_{in}/V_\Delta) \rightarrow 0$ . Thus,

$$\begin{aligned} T &= \frac{2V_\Delta}{\lambda} + \frac{A_{in}}{\lambda} \left\{ \sin\theta_0 - 2 \sin\left(\theta_0 + \omega_{in} \frac{V_\Delta}{\lambda}\right) + \sin\left(\theta_0 + \omega_{in} \frac{2V_\Delta}{\lambda}\right) \right\} \\ &= T_0 - \frac{A_{in}}{\lambda} \left\{ 1 - \cos\left(\omega_{in} \frac{T_0}{2}\right) \right\} \sin\left(\theta_0 + \omega_{in} \frac{T}{2}\right) \end{aligned}$$

where  $T_0$  is the unperturbed period of the oscillator. So,

$$F(\theta) = \theta + \omega_{in} T_0 - \frac{\omega_{in} A_{in}}{\lambda} \left\{ 1 - \cos\left(\omega_{in} \frac{T_0}{2}\right) \right\} \sin\left(\theta + \omega_{in} \frac{T}{2}\right) \pmod{2\pi} \quad (6.4)$$

The graph of  $F(\theta)$  is thus an oscillation superimposed on a ramp, with an offset of  $\omega_{in} T_0$ . The graphical solution to (6.1) is given in Fig.6.2(a). Equation (6.2) may be written as

$$T = 2T_1 + \frac{A_{in}}{\lambda} \left[ \sin(\theta_0 + \omega_{in} T) - \sin\theta_0 \right]$$

so that  $T$  can be obtained similarly, as in Fig.6.2(b). This process has to be repeated for all  $\theta_0$

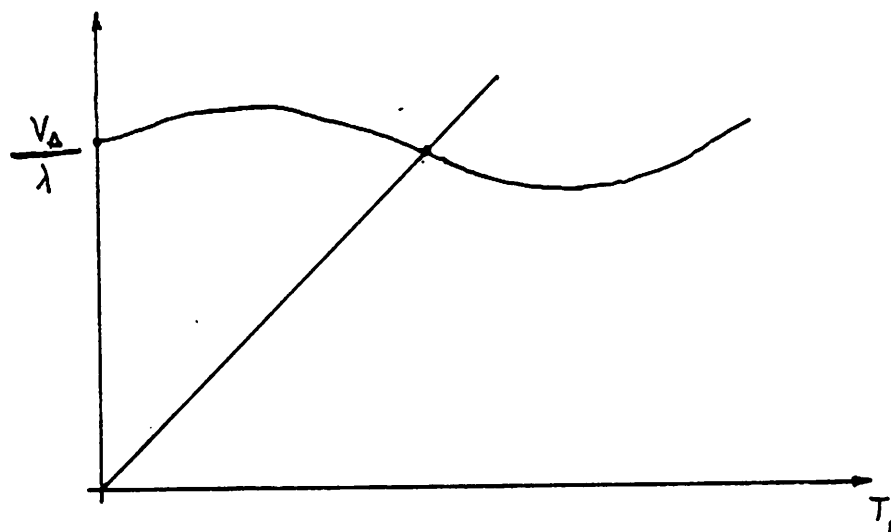


Fig. 6.2(a)

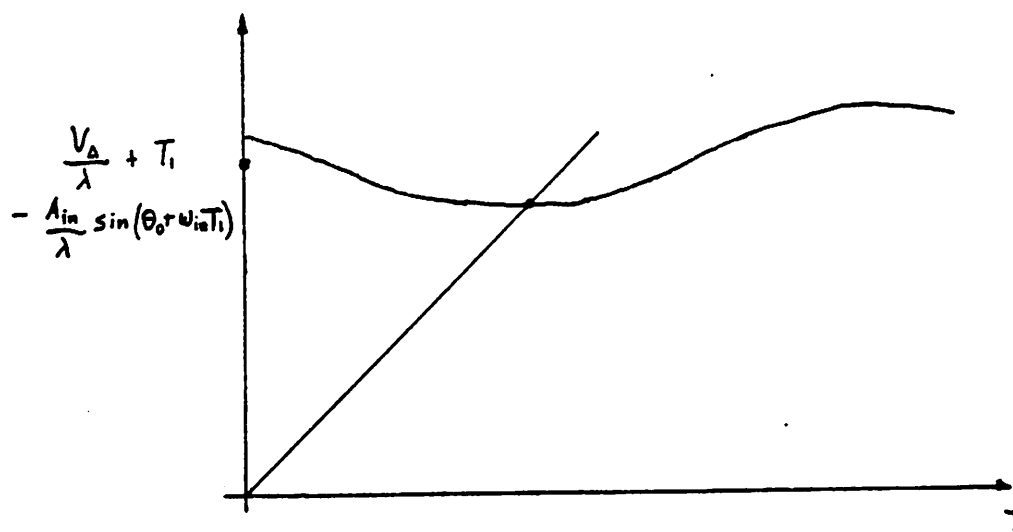


Fig. 6.2(b)

Graphical solutions to  $T_1$  and  $T$

in the interval  $[0, 2\pi)$ , so a graph of  $T$  vs.  $\theta_0$  is obtained (Fig.6.3). The magnitude of the oscillatory component is small compared to the offset, by the ratio of  $A_{in}$  to  $V_{\Delta}$ . A typical curve of  $F(\theta_0)$  vs.  $\theta_0$  is shown in Fig.6.4(a). The modulation of the oscillator from cycle to cycle is a discrete process which iteratively applies  $F(\cdot)$  to an initial phase  $\theta_0$ ; this is graphically represented in this figure as a rectilinear ray which successively reflects between the curve of  $F(\cdot)$  and the straight line of unit slope. We define  $\theta_0$  to be a *period  $k$  solution* of  $F(\cdot)$  if the ray closes upon itself after  $k$  reflections off the unit slope line. As an example, a period 3 solution is shown in Fig.6.4(b).

Various sorts of motion are possible in this dynamical system, and these are considered separately below.

*Case 1:  $\omega_{in}T_0 = 2(2n+1)\pi + \delta$ ,  $n = 0, 1, 2, \dots$  (small integers),  $\delta$  small*

This case corresponds to modulation by odd harmonics of  $T_0$ , and

$$F(\theta) = \theta + \delta + \frac{2\omega_{in}A_{in}}{\lambda} \sin\left(\theta + \frac{\delta}{2}\right) \quad (6.5)$$

as shown in Fig.6.5. There are two fixed points of  $F(\theta)$ ,  $\theta_1$  and  $\theta_2$ , where the first is globally stable and the second is unstable. Synchronisation occurs here, because  $\theta_1$  corresponds to a period 1 solution, with  $f_{in}$  different from  $f_{osc}$  by an amount proportional to  $\delta$ . The frequency of the oscillator is thus entrained by the periodic perturbation. This diagram also gives an estimate of the rate of entrainment, that is, the number of cycles which elapse between starting from an arbitrary initial condition to when the  $\theta$  is within a prescribed error away from  $\theta_0$ . This *cycle slipping* represents the transient of synchronisation, and is often an important consideration in system design.

*Case 2:  $\omega_{in}T_0 = 4n\pi + \delta$ ,  $n = 1, 2, 3, \dots$ ,  $\delta$  small*

This case corresponds to modulation by even harmonics, and

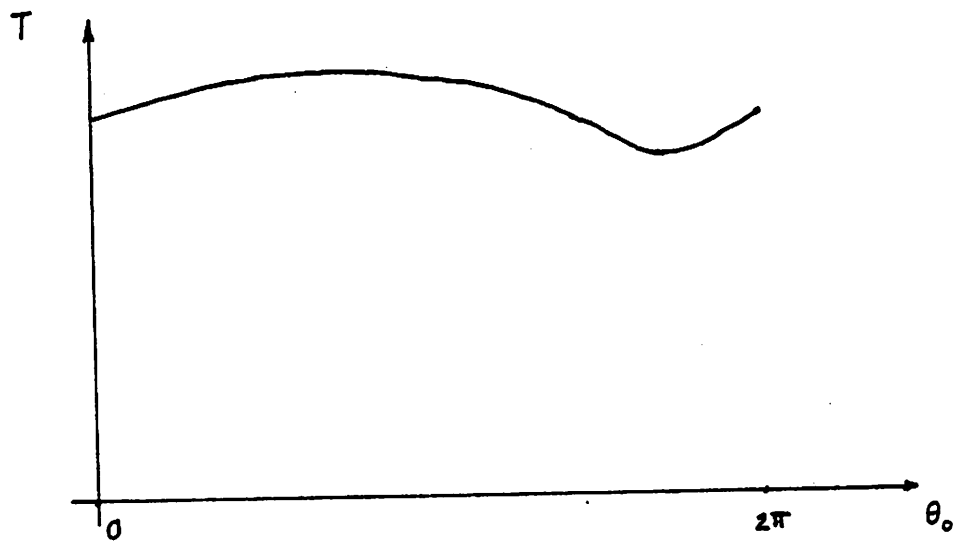
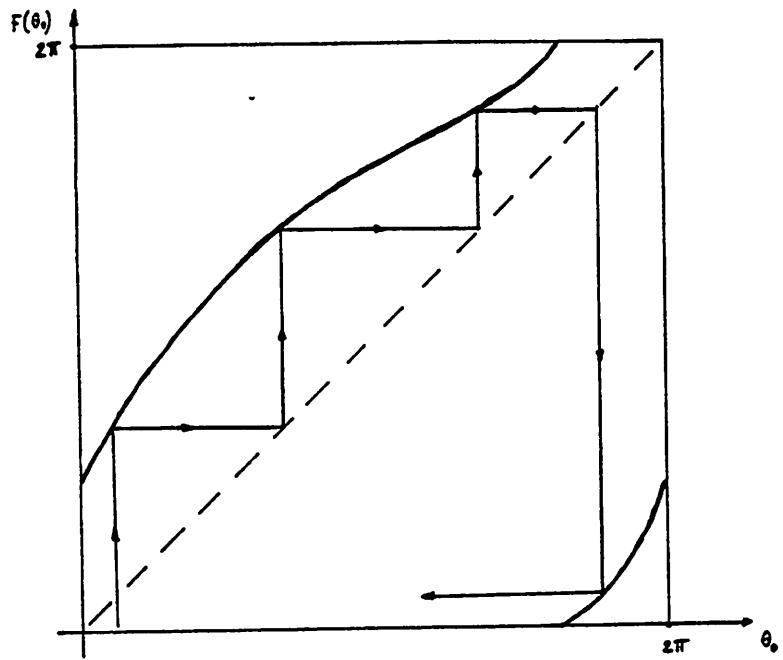
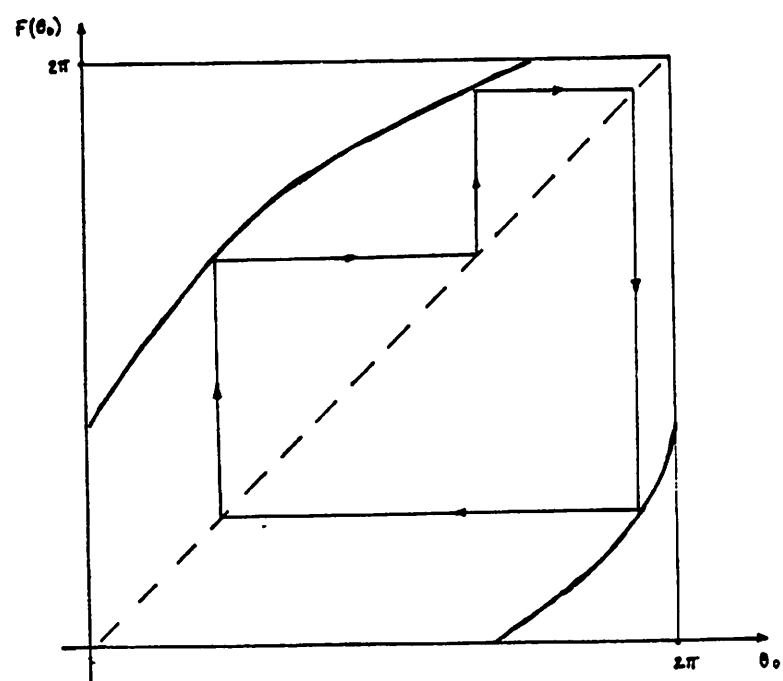


Fig. 6.3  
Graph of  $T$  vs  $\theta_0$



**Fig. 6.4(a)**  
A typical curve of  $F(\theta_0)$  vs.  $\theta_0$



**Fig. 6.4(b)**  
A period 3 solution

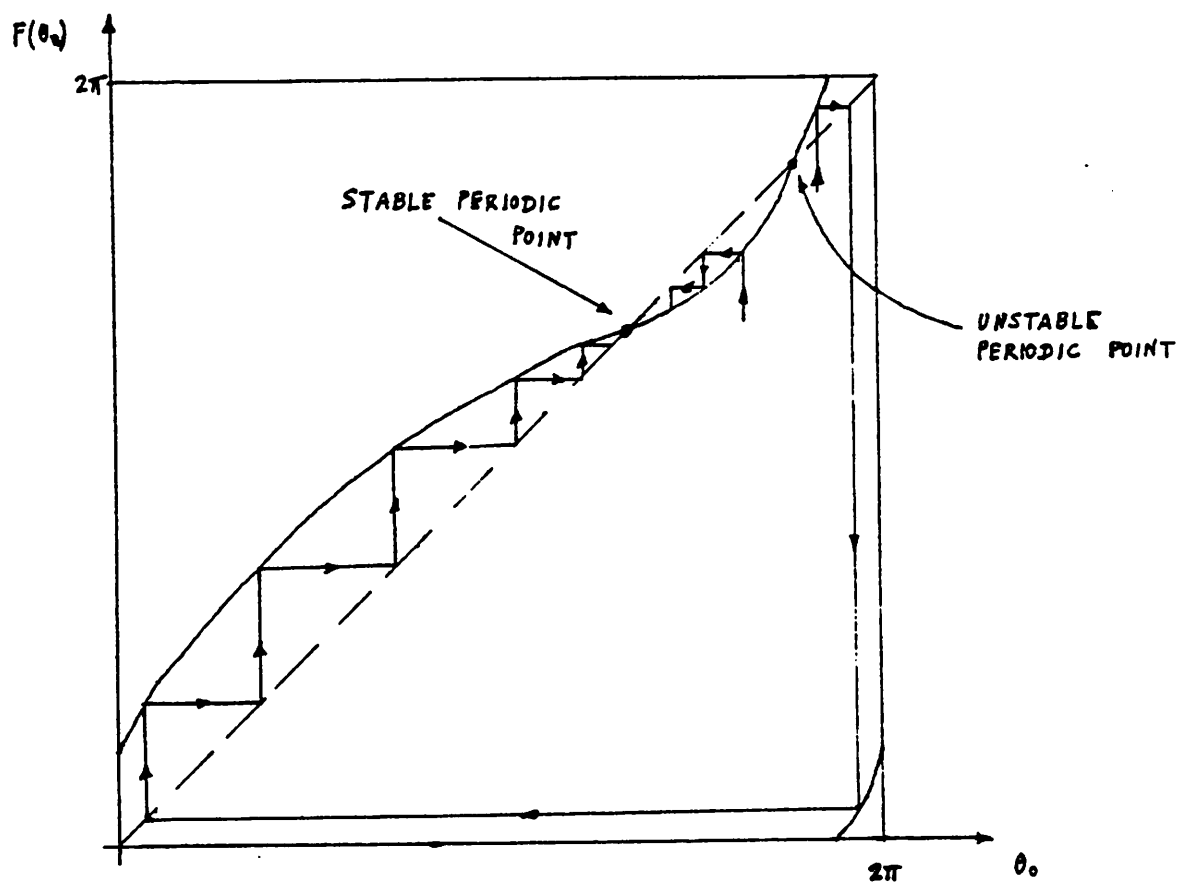


Fig. 6.5

A stable, and an unstable, period 1 solution

$$F(\theta) = \theta + \delta - o(\delta^2) \frac{2\omega_{in}A_{in}}{\lambda} \sin\left(\theta + \frac{\delta}{2}\right) \quad (6.6)$$

The important difference from the previous case is that the last term has a very small coefficient, so  $F(\theta)$  does not intersect the unit slope line, and no fixed point exists. This makes perfect sense when we consider an even harmonic of  $T_0$  as the modulation signal in Fig.6.1, which, by producing a cancelling modulation over each half cycle, cannot entrain  $T_0$ . The presence of the periodic signal does, however, influence the oscillator, as discussed in Case 3. In sum, then, odd harmonics can synchronise, and even ones cannot<sup>17</sup>; when synchronisation occurs, the capture range from Fig.6.5 is  $\pm \frac{2\omega_{in}A_{in}}{\lambda}$ .

*Case 3:  $\omega_{in}T_0 = 2n\pi + \delta$ ,  $n = 1, 2, 3, \dots$  (small integer),  $\delta$  large, and  $in \in [0, 2\pi)$ .*

This is, by far, the most likely case in practice.  $F(\theta)$  resembles the curves in Figs.6.4(a) and (b), so only higher order periodic solutions, or aperiodic ones, can exist. We now study the conditions for period  $k$  solutions, starting by way of a specific example.

Suppose  $A_{in} \rightarrow 0$  in (6.4), so that  $F(\theta)$  is a straight line (Fig.6.6). If a period 3 solution exists, the following must hold:

$$\begin{aligned} \theta_2 &= \theta_1 + \phi_0 \\ \theta_3 &= \theta_2 + \phi_0 \\ \theta_1 &= \theta_3 + \phi_0 - 2\pi \end{aligned} \quad (6.7)$$

which implies that

$$\phi_0 = \omega_{in}T_0 = \frac{2\pi}{3}$$

<sup>17</sup>The opposite may be true if the oscillator topology inverts the modulating signal over successive transitions every half cycle.



that is,

$$T_0 = \frac{T_{in}}{3}$$

In general, for a period  $k$  solution, we must have

$$\phi_0 = \frac{2\pi}{k} \cdot p \quad (6.8)$$

where the integer  $p < k$  is the number of times the phase has advanced by  $2\pi$  before repeating itself.

Therefore, if the amplitude of the perturbing signal is neglected completely, the intercept  $\phi_0$  is defined uniquely by the rational number  $p/k$ . If the amplitude  $A_{in} = \epsilon$ , a small number, then

$$F(\theta) = \phi_0 + \theta + \epsilon \sin(\theta + \phi_0)$$

Repeating the procedure of (6.7), except with a period  $k$  solution with initial condition  $\theta_0$ , we get

$$\theta_2 = \theta_1 + \phi_0 + \epsilon \sin(\theta_1 + \phi_0)$$

$$\theta_3 = \theta_2 + \phi_0 + \epsilon \sin(\theta_2 + \phi_0)$$

(6.9)

$$\theta_k = \theta_1 + 2p\pi = \theta_{k-1} + \phi_0 + \epsilon \sin(\theta_{k-1} + \phi_0)$$

Substituting for  $\theta_2$  to  $\theta_k$ , and ignoring terms of second or higher order in  $\epsilon$ , we obtain

$$\theta_1 + 2p\pi = k\phi_0 + \theta_1 + \sum_{i=1}^k \epsilon \sin(i\phi_0 + \theta_1)$$

This sum of this series can be written explicitly, giving

$$k\phi_0 - 2p\pi + \epsilon R_k \sin(\theta_1 + \Phi_k) = 0 \quad (6.10)$$

$$\text{where } R_k = \frac{2 \sin\left(\frac{k}{2} + 1\right) \frac{\phi_0}{2}}{\sin\left(\frac{\phi_0}{2}\right)} = 2 \text{ or } 2\cot\left(\frac{\phi_0}{2}\right) \text{ if } k \text{ is even or odd}$$

$$\text{and } \Phi_k = \arctan \left( \frac{\cos \frac{\phi_0}{2} \cos\left(\frac{k+1}{2}\right) \phi_0}{1 + \sin \frac{\phi_0}{2} \sin\left(\frac{k+1}{2}\right) \theta} \right)$$

If  $\phi_0 = \frac{2p\pi}{k}$ , then a *period k trajectory* exists with initial condition  $\theta_1 = \pi - \Phi_k$ . More importantly, though, if  $\phi_0$  is changed by a small amount, *this periodic solution will persist*, and the initial condition will change to

$$\theta_1 = -\Phi_k + \arcsin\left(\frac{k\phi_0 - 2p\pi}{\epsilon R_k}\right) \quad (6.11)$$

The range of permissible variation of  $\phi_0$  is

$$\Delta\phi_0 < \frac{\epsilon R_k}{k} \quad (6.12)$$

This illustrates the structural stability of the periodic solution, which means that its character is retained while some parameter is varied over a finite range.

The implications of this fact are interesting when we consider solutions of different periods. The period  $k$  solution defined by (6.10) can be uniquely associated with the rational number  $p/k$ ; let its associated lock range, determined by (6.12), be  $\Delta_{p/k}$ . Together, these define a unique open set on the interval  $[0,1)$  of the real line. As the rational numbers are dense on the real line, there always exists another rational  $p_1/k_1 \in \Delta_{p/k}$ , where  $k_1 > k$ . For the periodic solution of period  $k_1$  associated with this number, there is a capture range  $\Delta_{p_1/k_1}$  which defines an open set around it. Inside this open set is another rational number  $p_2/k_2$ ,

where  $k_2 > k_1$ . This process can be repeated *ad infinitum*.

For each choice of  $p_i/k_i$ , the associated  $R_{k_i}$  is either 2 or  $2 \cot(\frac{\phi_0}{2})$ , depending on whether  $p_i$  is even or odd; for small  $\epsilon$ , the value of  $R_{k_i}$  remains constant, independent of  $k_i$ . Let  $\bar{R}$  be the smaller of its two values. We choose

$$\Delta_{p_i/k_i} = \Delta_{p_{i-1}/k_{i-1}} \cap \left( \frac{p_i}{k_i} - \frac{\epsilon \bar{R}}{k_i}, \frac{p_i}{k_i} + \frac{\epsilon \bar{R}}{k_i} \right)$$

so that as  $k_i \rightarrow \infty$ ,  $\Delta_{p_i/k_i} \subset \Delta_{p_{i-1}/k_{i-1}} \subset \dots \subset \Delta_{p/k}$ . Being contained in nested subsets (Fig. 6.7), the sequence  $\{p_i \cdot pn + 2/k_i\}$  is then a Cauchy sequence, with an accumulation point  $\phi^*$ . Thus, if  $\omega_{in} = \phi^*$ , the solution could have one of infinitely many different periods. We state without proof that  $\phi^*$  is an irrational number, and the set of all  $\phi^*$  is densely spread out in the interval.

It is also possible for an initial condition to give rise to aperiodic solutions, which are generically classified as either *chaotic* [25], or *almost periodic* [26]. Investigating detailed properties of such solutions is a difficult task; their existence is established by considering how intervals are mapped into themselves under repeated applications of the map  $F(\cdot)$ . In the simple case when  $\epsilon$  is set to zero, an irrational value of  $\phi_0$  gives rise to almost periodic solutions.

Only those solutions which are locally stable can be observed experimentally. A periodic solution of period  $k$  with initial condition  $\theta_0$  is *locally asymptotically stable* if there exists a neighbourhood of  $\theta_0$ , such that for any  $\theta$  in this neighbourhood,  $|F^k(\theta) - \theta_0| < |\theta - \theta_0|$ . To ensure such stability, it is sufficient that  $|\frac{d}{d\theta} F^k(\theta)| < 1$ , which by the chain rule is equivalent to

$$\left| \prod_{i=0}^{k-1} \frac{d}{d\theta} F(\theta_i) \right| < 1 \quad (6.13)$$

where  $\theta_i = F^i(\theta_0)$  is the  $i^{\text{th}}$  iterate in the oscillation. In our case

$$\frac{d}{d\theta} F(\theta) = 1 - \epsilon \cos(\theta + \phi_0) \quad (6.14)$$

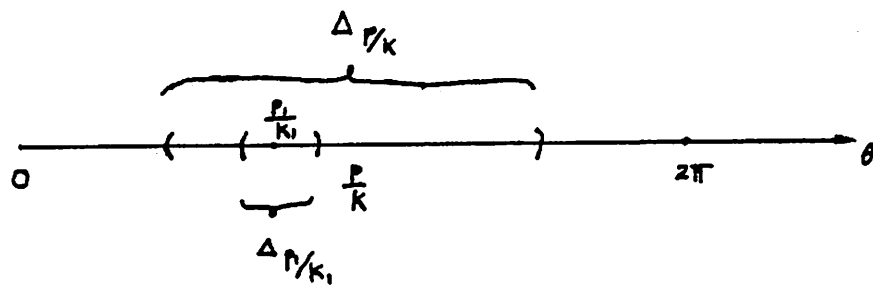


Fig. 6.7

Nested subsets

which is strictly greater than 1 when  $\theta \in [0, \frac{\pi}{2} - \phi_0] \cup [\frac{3\pi}{2} - \phi_0, 2\pi)$ . To satisfy (6.13), this requires that *all*  $k-1$  iterates of  $F(\theta)$  between one cycle of period  $k$  should be contained in this range. This never happens for small  $\epsilon$  for the case we are considering; however, note that this is only a sufficient condition, it might be possible to find a stronger one which can be verified.

A few remarks are in order concerning our  $F(\cdot)$ , when it is compared with the maps which are known to produce chaotic motions [25],[27]. The latter are non-monotonic continuous functions which map an interval into itself; ours, on the other hand, produces periodicity due to the *modulo*  $2\pi$  property of a phase angle. Strictly speaking,  $F(\cdot)$  maps a *meridian on the surface of a torus* into some shifted value of itself, rather than an interval on the real line. This torus is obtained by identifying opposite edges of the square  $[0, 2\pi) \times [0, 2\pi)$ , and an example of a "discrete" periodic trajectory on its surface is shown in Fig.6.8.

It should now be evident how complex the motions of a relaxation oscillator can be when it is subject to a periodic excitation. Under certain conditions, the solutions can have one of infinitely many periods, or be altogether aperiodic. Others can have periodic solutions of very large periods; often, when these are experimentally observed, they give the impression of being aperiodic as well. Figs.6.9(a) and (b) show, on the trajectories in the phase plane, the effects of modulation by low and high level periodic signals.



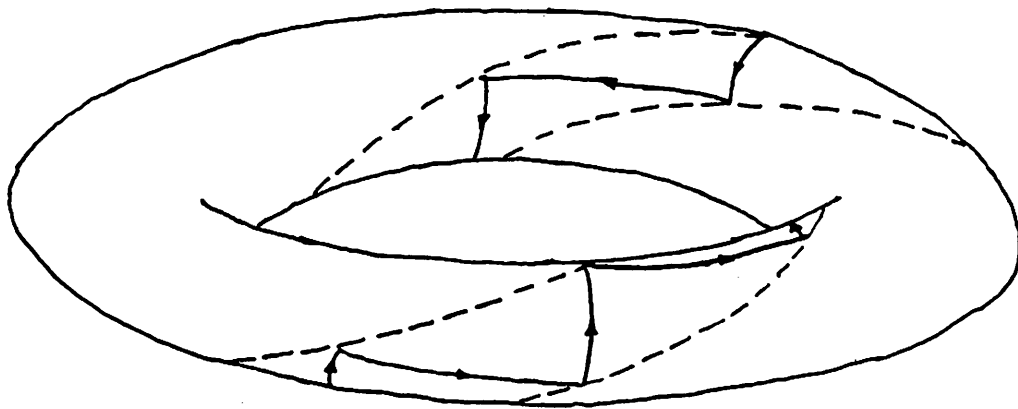


**Fig. 6.8**

**A discrete periodic trajectory on the surface of a torus**

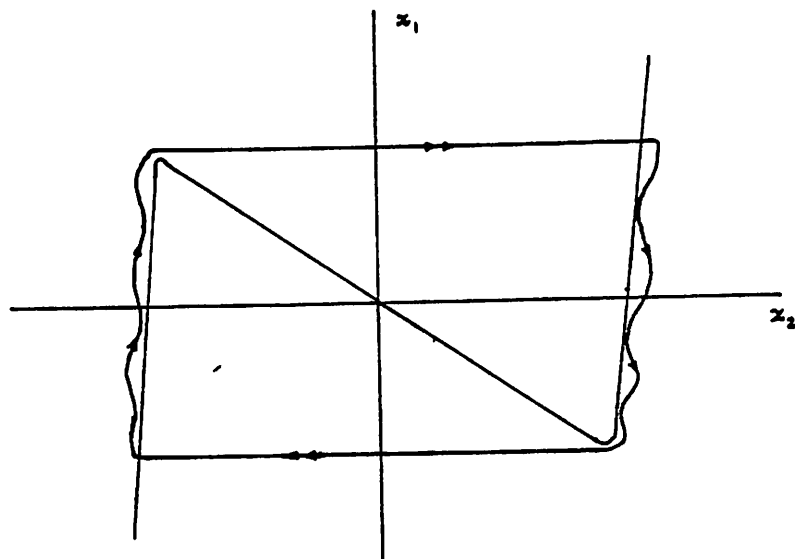


Fig. 6.9(a)

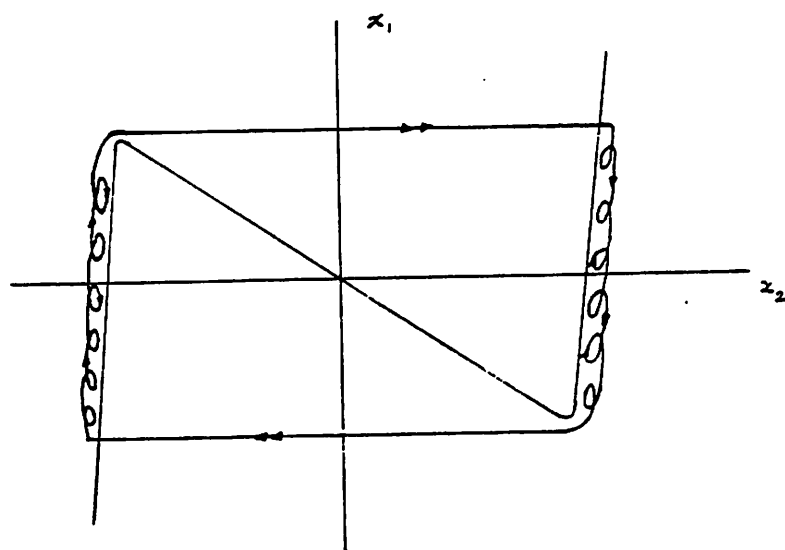


Fig. 6.9(b)

**Phase plane trajectories of a relaxation oscillator  
subject to periodic excitations of low and high amplitudes**

---

## References

- [1] van der Pol, B., Forced oscillations in a circuit with non-linear resistance, *Philosophical Magazine*, vol.3, pp.65-80, 1927.
- [2] Grebene, A.B., The monolithic phase locked loop - a versatile building block, *IEEE Spectrum*, vol.8, pp.38-49, March 1971.
- [3] Gilbert, B., A versatile voltage to frequency converter, *IEEE Journal of Solid State Circuits*, vol.SC-11, no.6, pp.852-864, December 1976.
- [4] Andronov, A.A. and S.E. Khaikin, *Theory of Oscillations*, Princeton University Press, Princeton, 1949.
- [5] Meyer, R.G., *Nonlinear Analog Integrated Circuits*, EE 240 class notes at U.C.Berkeley, 1976 (to be published).
- [6] Leeson, D.B. and G.F. Johnson, Short-term stability for a Doppler radar: requirements, measurements and techniques, *Proceedings of IEEE*, vol.54, no.2, February 1966.
- [7] Stewart, J.L., Frequency modulation noise in oscillators, *Proceedings of IRE*, vol.44, no.3, pp.372-376, March 1956.
- [8] Edson, W.A., Noise in oscillators, *Proceedings of IRE*, vol.48, no.8, pp.1454-1466, August 1960.
- [9] Mullen, J.A., Background noise in nonlinear oscillators, *Proceedings of IRE*, vol.48, no.8, pp.1467-1473, August 1960.
- [10] Golay, M.G.E., Monochromaticity and noise in a regenerative electrical oscillator, *Proceedings of IRE*, vol.48, no.8, pp.1473-1477, August 1960.

- 
- [11] Grivet, P. and A. Blaquiere, Nonlinear effects of noise in electronic clocks, *Proceedings of IEEE*, vol.51, no.11, pp.1606-1614, November 1963.
- [12] Eccles, W.H. and F.W. Jordan, A trigger relay utilising three electrode thermionic vacuum tubes, *Radio Review*, vol.1, pp.143-146, 1919.
- [13] Schmitt, O.H., A thermionic trigger, *Journal of Scientific Instrumentation*, vol.15, pp.24-26, January 1938.
- [14] Grebene, A.B. and H.R. Camenzind, Frequency selective integrated circuits using phase locked techniques, *IEEE Journal of Solid State Circuits*, vol.SC-4, pp.216-225, August 1969.
- [15] Black, H.S., *Modulation Theory*, van Nostrand, New York,
- [16] Inoue, S. and Y. Iso, Super high quality F.M. detector and its development process, *IEEE Transactions on Consumer Electronics*, vol.CE-24, no.3, pp.226-234, August 1978.
- [17] Thomas, J.B., *An introduction to Applied Probability and Random Processes*, Wiley, New York, 1971.
- [18] Sastry, S.S., C.A. Desoer and P.P. Varaiya, Jump behaviour of circuits and systems, Memo No. UCB/ERL M80/44, Electronics Research Lab., University of California, Berkeley, October 1980.
- [19] Middleton, D., Spurious signals caused by noise in triggered circuits, *Journal of Applied Physics*, vol.19, pp.817-830, September 1948.
- [20] Siegert, A.J.F., On the first passage time probability problem, *Physical Review*, vol.81, no.4, pp.617-623, February 15, 1951.
- [21] Levi, M., Qualitative analysis of periodically forced relaxation oscillations, Ph.D. thesis, New York University, 1978.

- 
- [22] Kukielka, J. and R.G. Meyer, A high frequency, temperature stable monolithic V.C.O., *ISSCC Digest of Technical Papers*, vol.XXIV, pp.126-127, 1981.
- [23] Buck, J. and E. Buck, Synchronous Fireflies, *Scientific American*, pp.74-85, May 1976.
- [24] Chillingsworth, D.R.J., *Differential Topology with a view to applications*, Pitman, London, 1976.
- [25] Li, T.-Y. and J.A. Yorke, Period three implies chaos, *American Mathematical Monthly*, vol.82, pp.985-992, December 1975.
- [26] Hale, J.K., *Ordinary Differential Equations*, Wiley, New York, 1969.
- [27] Ballieul, J., R.W. Brockett and R.B. Washburn, Chaotic motion in nonlinear feedback systems, *IEEE Transactions on Circuits and Systems*, vol.CAS-27, no.11, pp.990-997, November 1980.
- [28] Parzen, E., *Stochastic Processes*, Holden Day, San Francisco, 1962.

## Appendix 1

The standard deviation of the definite integral

$$y(T) = \int_0^T i_n(t) dt \quad (\text{A.1})$$

is to be calculated, where  $i_n(t)$  is white noise with a finite bandwidth. From [28], the distribution of  $y(T)$  is

$$W_1(y, T) = \frac{1}{\sqrt{2\pi K_y(T, T)}} \exp\left\{-\frac{y^2}{2 K_y(T, T)}\right\} \quad (\text{A.2})$$

which is Gaussian, with a variance of

$$K_y(T, T) \stackrel{\text{def}}{=} \int_0^T \int_0^T K_{i_n}(t_1, t_2) dt_1 dt_2 \quad (\text{A.3})$$

where  $K_x(t_1, t_2)$  is the co-variance kernel of the random variable  $x(t)$ .

For white noise with density  $\hat{i}$  A/ $\sqrt{\text{Hz}}$  and bandwidth  $\omega$  radians

$$K_{i_n}(t_1, t_2) = R(t) = \pi\omega \tilde{i}^2 \exp(-\omega |t|) \quad (\text{A.4})$$

where  $t = t_1 - t_2$  [28]. Integrating this as in (A.3), we have

$$\begin{aligned} K_y(T, T) &= \pi\omega \tilde{i}^2 \int_0^T \int_0^T \exp(-\omega |t_2 - t_1|) dt_1 dt_2 \\ &= 2\pi\omega \tilde{i}^2 \int_0^T \int_0^{t_2} \exp(t_2 - t_1) dt_1 dt_2 \\ &= 2\pi \tilde{i}^2 \left\{ T + \frac{e^{-\omega T} - 1}{\omega} \right\} = 2\pi \tilde{i}^2 T \end{aligned}$$

because  $T \gg \frac{1}{\omega}$  for typical values. Therefore,

---

---

$$\sigma \{y(T)\} = \sqrt{K_y(T, T)} = \sqrt{2\pi T} \hat{i} \quad (\text{A.5})$$

and the corresponding jitter is

$$\frac{1}{C} \sigma \{y(T)\} \cdot \frac{1}{V_\Delta} = \frac{\hat{i}}{I_0} \sqrt{\frac{2\pi}{T}} \quad (\text{A.6})$$

## Appendix 2

Using analogous methods to those in the text, we analyse the jitter due to a noise current,  $i_n$ , in an Emitter Coupled Oscillator made from generalised active devices and loads, as shown in Fig. A2.1.

The active devices have a transconductance specified by the function  $f_1(\cdot)$ , and the loads are voltage controlled resistors with characteristics  $f_2(\cdot)$ . For the circuit, then,

$$I_1 = f_1(V_2 - V_4) \quad (\text{A2.1})$$

$$V_2 = V_s - f_2(2I_0 - I_1) \quad (\text{A2.2})$$

$$V_1 = V_s - f_2(I_1) - I_n R \quad (\text{A2.3})$$

$$(2I_0 - I_1) = f_1(V_1 - V_3) \quad (\text{A2.4})$$

where  $R \stackrel{\text{def}}{=} \left(\frac{df_2}{dV}\right)^{-1}(I_1)$ , and is the incremental resistance applying to the small noise signal.

The capacitor determines the dynamics of the circuit:

$$C \frac{d}{dt} (V_3 - V_4) = I_0 - I_1 \quad (\text{A2.5})$$

Eliminating all the variables except  $I_1$  in (A2.1) to (A2.5), we get,

$$\begin{aligned} C \left[ -\frac{df_2(I_1)}{dI_1} - \frac{d}{dI_1} f_1^{-1}(2I_0 - I_1) + \frac{d}{dI_1} f_2(2I_0 - I_1) + \frac{d}{dI_1} f_1^{-1}(I_1) \right] \frac{dI_1}{dt} \\ = I_0 - I_1 - I_1 + C \frac{dI_n R}{dt} \end{aligned} \quad (\text{A2.6})$$

and re-arranging,

$$\frac{dI_1}{dt} = \frac{I_0 - I_1 + \frac{dI_n R}{dt}}{G(I_1)} \quad (\text{A2.7})$$

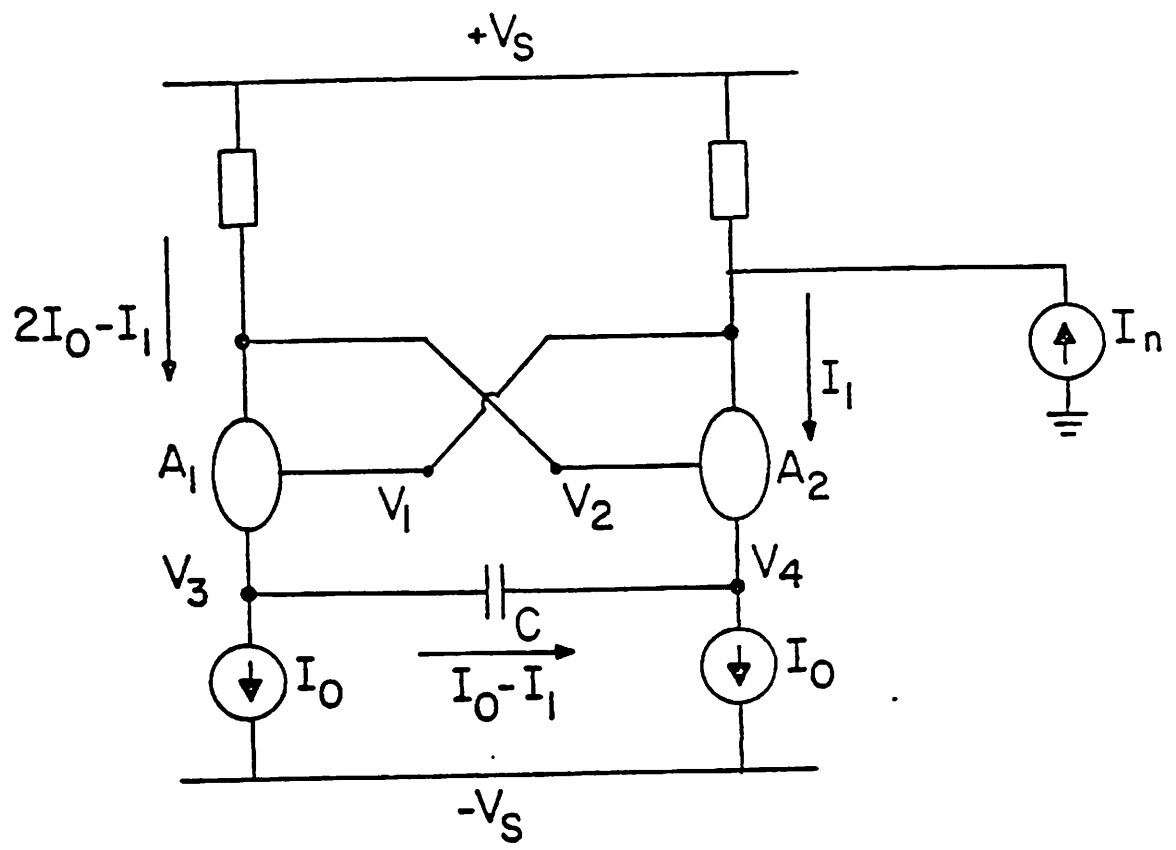


Fig. A2.1  
Generalised E.C.O.

where

$$G(I_1) \stackrel{\text{def}}{=} -\frac{df_2(I_1)}{dI_1} - \frac{d}{dI_1} f_1^{-1}(2I_0 - I_1) + \frac{d}{dI_1} f_2(2I_0 - I_1) + \frac{d}{dI_1} f_1^{-1}(I_1)$$

If the circuit is to oscillate, there must exist some  $I_1 \in (0, I_0)$  such that  $G(I_1) = 0$ ; this is the regeneration point. In turn, this requirement places restrictions on the functions  $f_1(\cdot)$  and  $f_2(\cdot)$ .

Consider now the timing cycle of the oscillation from  $t = t_A$ , when  $I_1 = I_A$ , to  $t = t_R$ , when  $I_1 = I_R$ . Integrating (A2.7),

$$\int_{I_A}^{I_R} G(I_1) dI_1 = \int_{t_A}^{t_R} \left[ \frac{I_0}{C} - \frac{I_1}{C} + Rj_n \right] dt$$

so

$$\frac{I_0(t_R - t_A)}{C} - \int_{t_A}^{t_R} \frac{I_1}{C} dt + R [I_n(t_R) - I_n(t_A)] = V_k \quad (\text{A2.8})$$

$$\text{where } V_k \stackrel{\text{def}}{=} \int_{I_A}^{I_R} G(I_1) dI_1$$

and  $V_k$  depends only on device parameters.

Equation (A2.8) specifies the variations in  $t_R$  due to the noise  $I_n$ ; if these variations are small compared to the relaxation time, we can write (A2.8) as

$$\frac{I_0 - I_{1R}}{C} T + RI_n(t) = V_k \quad (\text{A2.9})$$

where  $T \stackrel{\text{def}}{=} t_R - t_A$ ,  $I_{1R} \stackrel{\text{def}}{=} I_1(t_R)$  and  $I_n(t_A)$  is ignored because noise during relaxation is unimportant when we are concerned with the uncertainty in the instant of a *single* transition.

Consisting of a ramp crossing a noisy threshold, this is precisely the same result as for the bipolar transistor circuit in CHAPTER 3.